Proton Treatment Planning

3

Chuan Zeng, Richard A. Amos, Brian Winey, Chris Beltran, Ziad Saleh, Zelig Tochner, Hanne Kooy, and Stefan Both

Contents

C. Zeng
Procure Proton Therapy Center, Sumerset, NJ, USA
e-mail: chuan.zeng@nj.procure.com

R.A. Amos
University College London, London, UK
e-mail: r.amos@ucl.ac.uk

B. Winey • H. Kooy
Department of Radiation Oncology, Massachusetts General Hospital, Boston, MA, USA
e-mail: Winey.Brian@mgh.harvard.edu; HKOOY@mgh.harvard.edu

C. Beltran
Mayo Clinic, Rochester, MI, USA
e-mail: Beltran.Chris@mayo.edu

Z. Saleh
Memorial Sloan-Kettering Cancer Center, New York, NY, USA
e-mail: SalehZ@mskcc.org

S. Both (✉)
Department of Radiation Oncology, University Medical Center Groningen, Groningen, The Netherlands
e-mail: s.both@umcg.nl

Z. Tochner
University of Pennsylvania, Philadelphia, PA, USA
e-mail: Zelig.Tochner@uphs.upenn.edu

N. Lee et al. (eds.), *Target Volume Delineation and Treatment Planning for Particle Therapy*, Practical Guides in Radiation Oncology,
https://doi.org/10.1007/978-3-319-42478-1_3

3.1 Differences Between Photon and Proton Treatment Planning

The differences between planning proton-beam therapy and photon-beam therapy derive from the differences in the physics of protons and photons, namely [1]:

- That protons have a finite and controllable (through choice of energy) penetration in depth with virtually no exit dose (Fig. 3.1).
- That the penetration of protons is strongly affected by the nature (e.g., density) of the tissues through which they pass, while photons are much less affected (density changes generally give rise to only small intensity changes, except for the lung). Therefore, heterogeneities are much more important in proton-beam therapy than in photon-beam therapy (Fig. 3.2).

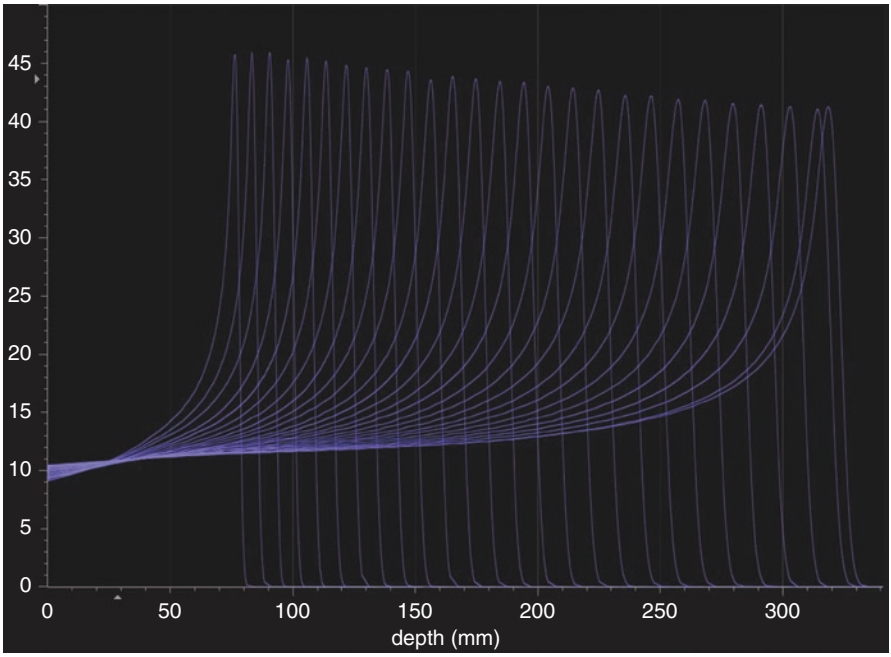

Fig. 3.1 Example integrated depth dose curves (arbitrary unit) corresponding to proton beams with different energies (100–230 MeV). Beams with higher energies penetrate deeper

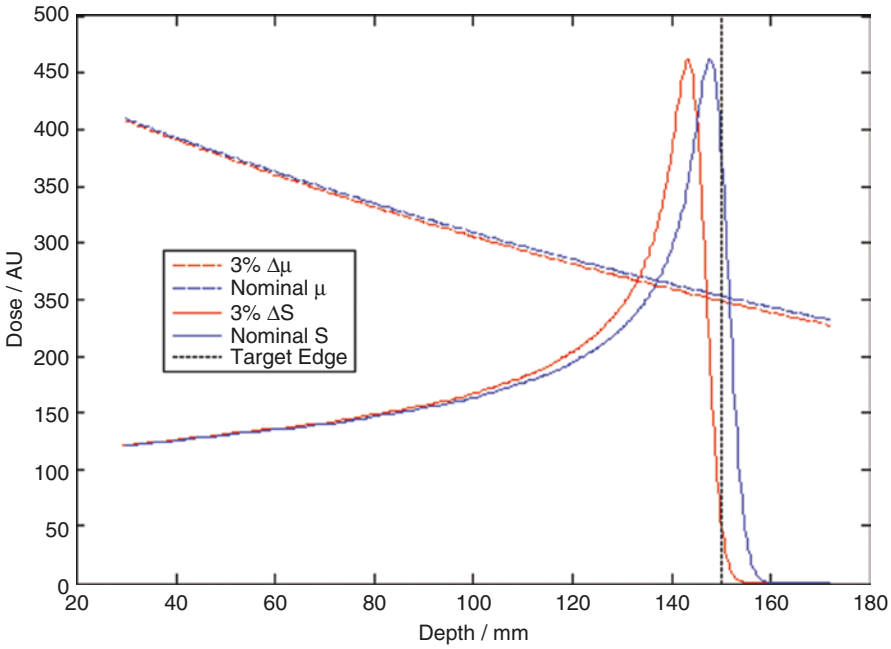

Fig. 3.2 Effect of a 3% increase in the attenuation parameters—stopping power for proton and attenuation coefficient for photon—on the proton and photon field. Note that the proton field shift causes a full underdose at the target edge, while the photon field is minimally affected

- The apparatus for proton-beam delivery is different, and its details affect the dose distributions (Chap. 2).

3.1.1 Physics

3.1.1.1 Rationale for Proton Therapy

Advantage of proton therapy comes from the physical characteristics of the proton beam:

- Finite range and ability to define depth of penetration.
- Intrinsic 3D shaping feature, in depth and laterally, compared to the 2D lateral controls in a single photon beam.
- Inserting a material of certain thickness in a proton beam results in a proportional energy reduction (range $\propto$ energy1.77; [2]) and a known shift downward of the range; proton-beam intensity *does not* change (in contrast to a clinical photon beam where the mean energy is minimally affected while the intensity reduces exponentially as a function of thickness).
- Intrinsically sharp penumbral edge due to near-straight tracks of protons (intrinsically sharper compared to a single photon-beam penumbra at depths below $\sim$ 18 cm in water).
- Proton beams deposit virtually no dose beyond the distal edge of the Bragg peak. Photon beams, in contrast, have no localization ability along the depth and "pass" throughout the patient. This simple difference means that a composite of multiple proton beams will have approximately half the integral dose of a similarly arranged set of photon beams [3].
- Proton dose distributions are biologically equivalent to photon dose distributions except for a constant RBE factor of 1.1 (more detail later in the chapter; Table 3.1).

3.1.1.2 Heterogeneities

Because of the influence of heterogeneities, a map of heterogeneities along the beam path must be made and compensated for (to the extent feasible); finally, the dose distributions must reflect the remaining effects of the heterogeneities. The map of heterogeneities is built up from fine-resolution CT images converted to water-equivalent densities in order to compute three-dimensional dose distributions.

The resulting requirements for planning proton-beam therapy imply the following [1]:

- To ascertain the CT number to water-equivalent density conversion table
- To compensate, either physically or virtually, for heterogeneities, including metallic implants when present
- To be aware of, and mitigate the effect of, possible hot and cold spots due to lateral scattering effects
- To take into account uncertainties associated with possible misalignment of the compensator (Chap. 2) with the patient's tumor, organs, and tissues for passive scattering proton therapy
- To take into account uncertainties in proton-beam penetration. For example, it is common practice to partially or completely avoid using beam directions for

Table 3.1 Major sources of uncertainty in proton therapy

Source of uncertainty	Comments
Range uncertainty	Proton-beam range varies as a function of proton energy and relative stopping power (RSP) of the absorbing material. A significant source of range uncertainty comes from the conversion of Hounsfield units (HU) in the planning CT to RSP (Fig. 3.4a). This uncertainty is approximately 2% for soft tissue and as high as 5% for lung, fat, and bone. An average value of 3.5% is assumed for clinical practice [4–6]. Much greater uncertainty exists for high-Z materials such as metal hip prostheses (Fig. 3.11) and dental fillings. Traversing these implants should be avoided wherever possible. CT image reconstruction artifacts also increase range uncertainty [7]
Patient setup uncertainty	Proton dose distributions are highly sensitive to patient positioning. Daily image guidance is recommended to ensure accurate alignment with the machine isocenter as well as alignment of patient relative to the patient support system and immobilization equipment traversed by the proton beams [8, 9]
Anatomical variability	Protons are highly sensitive to intrafractional and interfractional variations in anatomy. Variations may be caused, for example, by respiratory motion, weight loss, tumor shrinkage (Fig. 3.14), bladder filling, bowel gas, or changes in sinus filling. Mitigation techniques include 4D CT-based planning for respiratory motion, adaptive replanning for weight loss or tumor shrinkage, and careful beam angle selection to avoid traversing anatomy susceptible to variation wherever possible
Biological uncertainty	The relative biological effectiveness (RBE) is accepted as 1.1 for clinical practice. This is based on a meta-analysis of in vivo and in vitro data obtained in the middle of the SOBP [10]. However, linear energy transfer (LET) increases toward the distal end of the SOBP, with a corresponding increase in RBE [11]. The biological dose is extended distal to the physical range [12]; 2–3 mm is a reasonable approximation for this extension

which there would be a tight margin between the target and a sensitive structure lying distal to it (e.g., the spinal cord)

3.1.2 Geometric Uncertainties, Range Uncertainty, and the PTV Concept

The primary physical and conceptual difference between protons and photons passing through matter is that protons lose energy but not intensity and photons lose intensity but not energy (Sect. 1.1). An uncertainty in tissue density thus has a direct effect on the proton penetration and the position of the Bragg peak. If this Bragg peak was assumed to be at the distal edge of the target, it may "stop short" and the target edge may receive zero dose due to the sharp distal falloff of the Bragg peak. Figure 3.2 illustrates the effect on a proton Bragg peak with respect to the target and the effect on a photon field both for a 3% increase in the relevant physical attenuation parameter.

The difference in consequence is the root cause of the difference in uncertainty mitigation strategies between protons and photons.

As can be seen in Fig. 3.2, the photon field intensity and thus dose is minimally impacted by changes in density. As a consequence, a photon dose distribution has (almost certainly within the range of uncertainties of therapy) a static 3D shape in the patient space unaffected by acceptable uncertainties. This means that if we are

able to position the patient with respect to this static 3D shape, we will achieve our intended doses within the patient. This is the sole reason why geometric imaging suffices in photon radiotherapy: we only need to shift the patient to the intended location to align with the 3D dose. Any residual uncertainties are accounted for by PTV margin, to ensure that the CTV within remains covered.

The proton dose distribution is a composite of numerous pristine Bragg peaks whose terminal locations are the main loci of dose. Uncertainty in stopping power translates into a proportional uncertainty in all these loci. This direct correlation between geometric error and dose error (unlike in photon fields) means that an expansion of the CTV into a PTV does not apply directly to protons.

Uncertainties arise from:

1. Uncertainty in local stopping power in the patient
2. Changes in the patient's internal and external anatomy
3. Setup errors

   All causes have the same effect: a potential shift of the Bragg peak location. Stopping power uncertainties arise from (1) the conversion of CT number to stopping power based on a population average conversion curve and (2) the inherent uncertainty in the stopping power itself. Typically, the practical uncertainty in this conversion is assumed to be about 2.5%, which can vary from one institution to another (values up to 3.5% are used in clinical practice). Thus, a 150 mm range proton may have its (worst case) locus between 146.25 mm and 153.75 mm, i.e., an uncertainty range of 7.5 mm, which would be unacceptable.

   Changes in the patient's internal and external anatomy require repeated verification volumetric imaging depending on the treatment site. Over the course of treatment, the anatomy of the patient can change. Weight gain/loss is a typical example where thickness of a patient's subcutaneous fat layer may change significantly during the course of radiotherapy. Changes in the size of a bulky tumor or lymph nodes can affect the delivered dose. Gas in the rectum or bowels can create large perturbations if the proton beam is traversing these areas. The repeated image set should be used to reassess the dose to the patient as apparent geometric fidelity may *not* translate into dosimetric fidelity. This can be practically checked on a biweekly basis.

Daily imaging, either minimally by means of orthogonal X-rays or maximally by cone beam CT (CBCT) or diagnostic quality CT, is required to ensure that patient setup errors are within tolerances and representative of the assumed errors.

The known effect of uncertainties yet their unknown magnitude in a given patient requires mitigation at the treatment planning level to ensure that the resultant dose distribution maintains its integrity, qualitatively expressed as robustness against those uncertainties, in the presence of these uncertainties.

Robustness assessment is a difficult computational and practical problem and depends on the mode of proton field delivery. We identify two practical modes of delivery and their mitigation:

1. SOBP fields composed of a fixed set of pristine Bragg peaks with a fixed modulation and shaped by apertures in the lateral dimensions and by range compensator in depth. To the first order, an uncertainty shifts the field proportional

to the uncertainty. Thus, an expansion of the SOBP field in the proximal and distal directions will ensure proximal and distal coverage. This can be considered as a one-dimensional PTV expansion. An aperture expansion, to first order similarly, will ensure that the target remains covered in the lateral dimensions barring large heterogeneity differences. Note, however, that the first mitigation along depth is because of stopping power uncertainty, while the second is because of setup error. In addition, lateral setup errors are, in practice, corrected by assuming a worst case penetration in the shape of the range compensator (see Fig. 3.3).

2. PBS (pencil-beam scanning) fields composed of individual Bragg peaks. We identify two modes for PBS (nomenclature is not uniform in the radiotherapy community, and we follow the ICRU Report 78 [1]):
   (a) Single-field uniform dose (SFUD) where each field in the set of PBS fields achieves a uniform dose over the entire target. The fields are thus geometrically decoupled and can be considered independently in the uncertainty mitigation. Their individual mitigation is considered adequately handled by the considerations in SOBP fields. The SFUD technique is also called single-field optimization (SFO). The SFO may be used in the case of a simultaneous integrated boost (SIB) or when a single field is optimized together with constraints to OARs which partially overlap with the target.

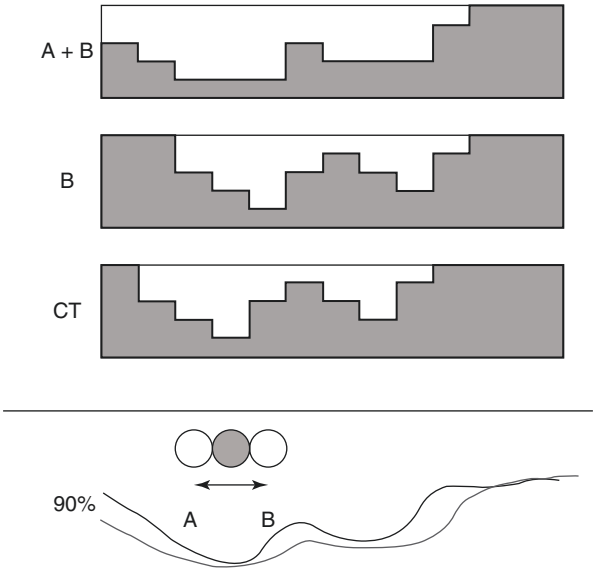

Fig. 3.3 Consider a beam entering from the top of the three range compensators. The range compensator "CT" is derived from the CT in the nominal position and has a profile as indicated and results in the top 90% dose profile. A setup error (e.g., to location B) results in a shifted compensator profile. The worst case range compensator profile (A + B, where A refers to the setup error to opposite direction of B) considers the deepest required penetration anywhere in the field given the range of uncertainties and results, as a consequence, a nominally deeper 90% dose profile

(b) Intensity-modulated proton therapy (IMPT) where each field delivers a heterogeneous dose to the target and only the composite dose from all fields covers the entire target and achieves the desired dose shape. The IMPT fields are strongly coupled and must be considered as a single set in the uncertainty mitigation. The uncertainty mitigation in IMPT may be achieved through robust optimization, which requires an explicit computation of individual uncertainty scenarios to assess that the dose in each scenario remains clinically acceptable. We will return to this topic in Sect. 6.4. The IMPT technique is also referred to as multi-field optimization (MFO) (Table 3.2).

3.1.3 Particularities of the Delivery System Proton Versus Photon

3.1.3.1 Proton Delivery Techniques

In proton-beam therapy, a number of different beam-shaping and delivery techniques can be used, and these techniques strongly affect the selection of beams and their resulting dose distributions [1]. The planning software must therefore be able to simulate all techniques of proton-beam delivery available to the user. For example, it might be required to compute the dose distributions of scatter beams, scanned beams (continuous or discrete), or wobbled beams (a special case of beam scanning, using relatively wide finite pencil beams):

- Protons have a sharp lateral beam penumbra which decreases with increasing beam energy.
- Proton-beam penumbra is widest in the Bragg peak region where the proton energy is least.

Table 3.2 Proton delivery techniques

Passive scattering	Pencil-beam scanning
An SOBP field is of constant modulation, thus in general *cannot* conform to the proximal volume of target	The dose distribution of one field can conform to the volume proximal to the target
The width of SOBP is determined by the widest part of the target in depth	The width of SOBP is determined by the width of the target in depth along each line of spots
Dose distributions are determined laterally by the collimation system	Dose distributions are determined laterally by the placement and weights of the spots on each energy layer
Penumbra will be affected by the air gap between the aperture and patient	Penumbra is largely determined by size of spot perpendicular to the beam direction and distance between range shifter (if any) and patient
Field size is usually limited. The limit may depend on range/modulation due to the different hardware options involved for different range/modulation combinations	

- Penumbra is narrower for protons compared to photons for depths of penetration less than 17–18 cm (This is the result of proton interaction with tissue, which is independent of delivery technique.).

3.2 Proton-Specific Treatment Simulation and Immobilization Principles

CT simulation is mandatory for proton therapy and it provides:

- 3D and/or 4D model of patient for geometric treatment planning
- Reference images for daily treatment guidance
- Material composition information, specifically proton stopping power, for heterogeneity corrections and substrate for dose distribution calculation

The processes of simulation and immobilization are essential when advanced technologies are employed in conjunction with tight treatment margins. In general, the use of tighter margins is employed to protect normal tissues and requires precise knowledge regarding geometric uncertainties (patient setup, motion, etc.) in radiation therapy.

The data on geometric uncertainties established in conventional external beam is of similar value to charged particle radiotherapy. However, the additional challenges of range uncertainty in particle therapy, a dimension in patient positioning not present in photon radiotherapy, raise a new challenge for particle therapy:

- Proton therapy demands repeatable, reliable simulation to successfully leverage the advantages of very selective dose distributions.
- Robust treatment planning can help accommodate a small amount of variation.
- Proton plans are highly susceptible to deterioration due to interference between the proton beam and the immobilization equipment.

The whole process of simulation and immobilization includes patient preparation, patient positioner (typically 6D), patient position verification system, patient immobilization, and patient imaging (preferably 3D).

3.2.1 CT Protocol, 4D CT, DIBH, DECT, and Contrast/Non-contrast CT

CT images are used to map the patient anatomy in terms of proton stopping power ratio properties. The accuracy in estimating the stopping power ratio from CT numbers is critical, and stoichiometric calibration, described below, is typically used to minimize range uncertainties due to CT imaging [13, 14]. This method has the advantage of not being affected by the differences in elemental composition between substitute material used in calibration and actual biological tissues. However,

stoichiometric calibration does not eliminate the uncertainty in estimated stopping power ratios; and imaging is not the only source of range uncertainty.

As a consequence, a distal margin of approximately 2.5–3.5% of the range is usually taken into account during planning. This uncertainty can perhaps be reduced using DECT [15], proton radiography [16], etc. In general:

- 3D and 4D CT-based simulations are standard in particle therapy.
- Use only calibrated protocols corresponding to particular kVp, since CT numbers are dependent on kVp.
- Scanner-specific calibration is recommended.
- The planning CT should fully include the immobilized patient.
- Treatment table and all immobilization equipment need to be included in the planning CT.
- The CT field of view must include all materials that are potentially in the beam's path.
- Setup reproducibility is paramount; therefore, indexed immobilization devices should be employed.
- CT artifacts and contrast materials are of concern and should be minimized or corrected as necessary.

3.2.1.1 Stoichiometric Calibration [13]

The error of relative stopping power distribution originates from a number of sources. Firstly, the measurement of CT number of homogeneous material can vary between 1% and 2% and is also dependent on the location of the material in the image, a variation that can reach up to 3%. In addition, the measurement of high CT numbers can vary from scanner to scanner and can strongly influence the calibration. It is also known that scanner-specific parameters such as the scan diameter and the matrix size may affect the measurement of CT number. A final source of error is the approximation of real tissue with tissue substitutes used for the measurement of the relationship of CT number to stopping power. The chemical composition of commonly used tissue substitutes is different to that of real tissue. A possible solution to this problem is a stoichiometric calibration:

1. Acquire CT scan of phantom with tissue equivalent materials with known relative electron density and elemental compositions (Figs. 3.5 and 3.6).
2. Measure CT numbers for each tissue equivalent material.
3. Use measured CT numbers to determine coefficients k^{ph}, k^{coh}, and k^{KN} for stoichiometric equation

$$\mu = (\langle Z^{3.62} \rangle_e k^{\mathrm{ph}} + \langle Z^{1.86} \rangle_e k^{\mathrm{coh}} + k^{\mathrm{KN}}) \rho N_A Z/A,$$

where chevrons $\langle \rangle_e$ denote an average weighted by number of electrons (Fig. 3.4).
4. Using coefficients to calculate CT numbers for a full range of "real" tissues using their published elemental compositions and physical densities [17, 18].

5. Calculate the stopping power ratio for each "real" tissue based on elemental composition (Bethe formula).
6. Use calculated SPR versus calculated CT numbers to establish respective calibration for TPS.
   The overall accuracy of the range control of proton beams in the human body by using this stoichiometric calibration was estimated to be 1.8% and 1.1% for bone and soft tissue, respectively [14].

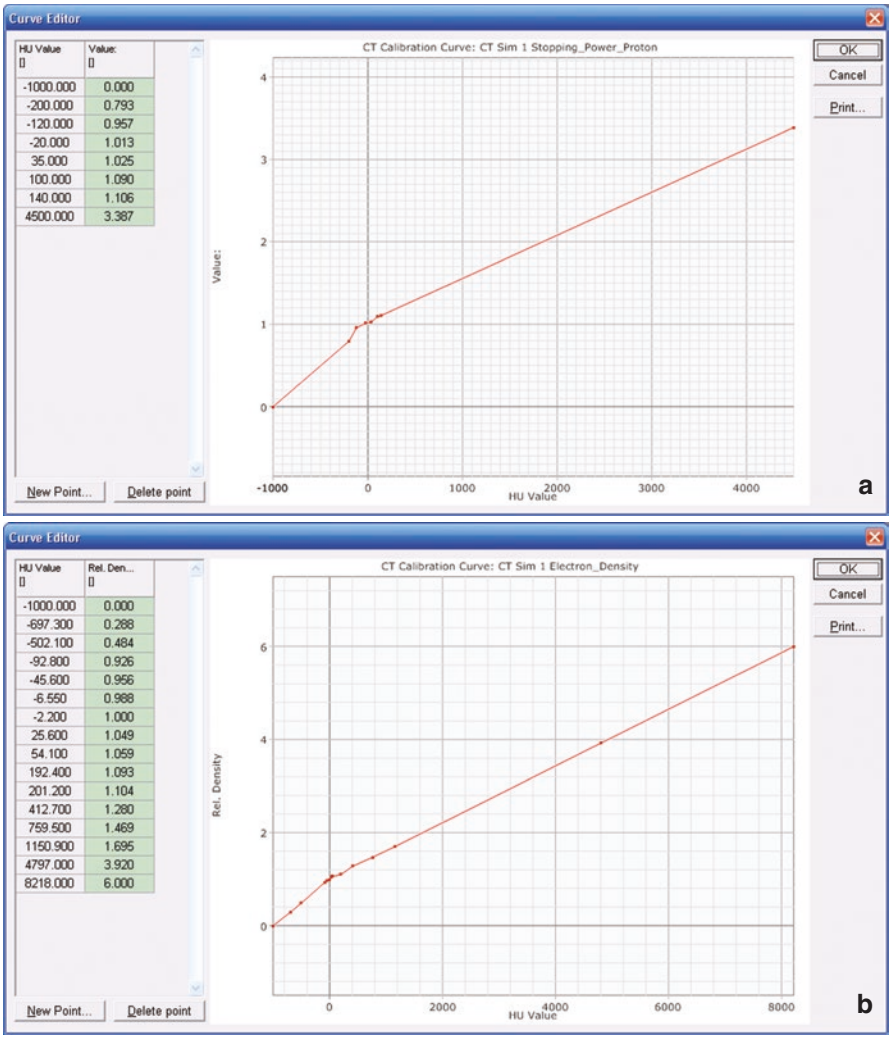

Fig. 3.4 Example CT calibration curves for proton stopping power ratio (**a**) and relative electron density (**b**). Hospital of the University of Pennsylvania (SIEMENS Sensation Open; 120 kVp)

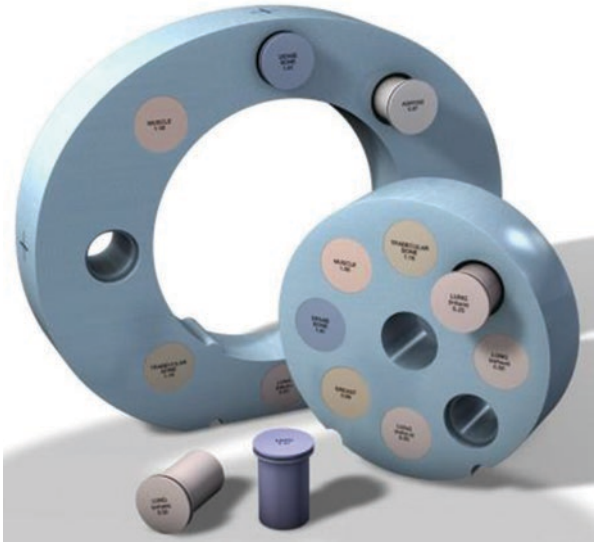

Fig. 3.5 CIRS electron density phantom (Courtesy of Computerized Imaging Reference Systems, Inc.)

3.2.1.2 DECT [15]

Schneider et al. [19] have demonstrated that a single CT number cannot differentiate between a change in density or chemical composition of an imaged material. Dual-energy CT (DECT), however, is able to attribute changes in X-ray attenuation to either density or chemical composition. This is achieved by decomposing two simultaneous single-energy CT (SECT) scans into relative electron density and effective atomic number. The process exploits the energy dependency of kilovoltage X-ray interaction atomic cross sections and the energy-independent parameter. The extra information gained in DECT, compared to SECT, can be used to estimate two material-specific parameters, and these are then used in a direct calculation of the SPR instead of a fitted value as in the stoichiometric method. The use of DECT has been shown to reduce the range uncertainty in PT compared to SECT [20]:

- DECT has the potential to better characterize patient composition and stopping power.
- Reduce SPR uncertainties from 1.1 (SECT) to 0.4% for soft tissue [21] and from 13 to 3% for a silicone-based dosimeter [22].
- Reduce maximum dose calculation error from 8 to 1% [23].

3.2.1.3 CT Contrast Avoidance [24]

- The use of contrast agents is common in CT studies employed in treatment planning.
- Contrast agents accumulate, and their iodine content increases the CT number of soft tissues significantly, creating artifacts and degrading the quality of CT images.
- Whenever a contrast agent is needed for target delineation purposes, the contrast CT has to be acquired after a simulation CT is acquired without contrast.
- Treatment planning calculations must be done on the non-contrast CT scan to avoid significant range errors

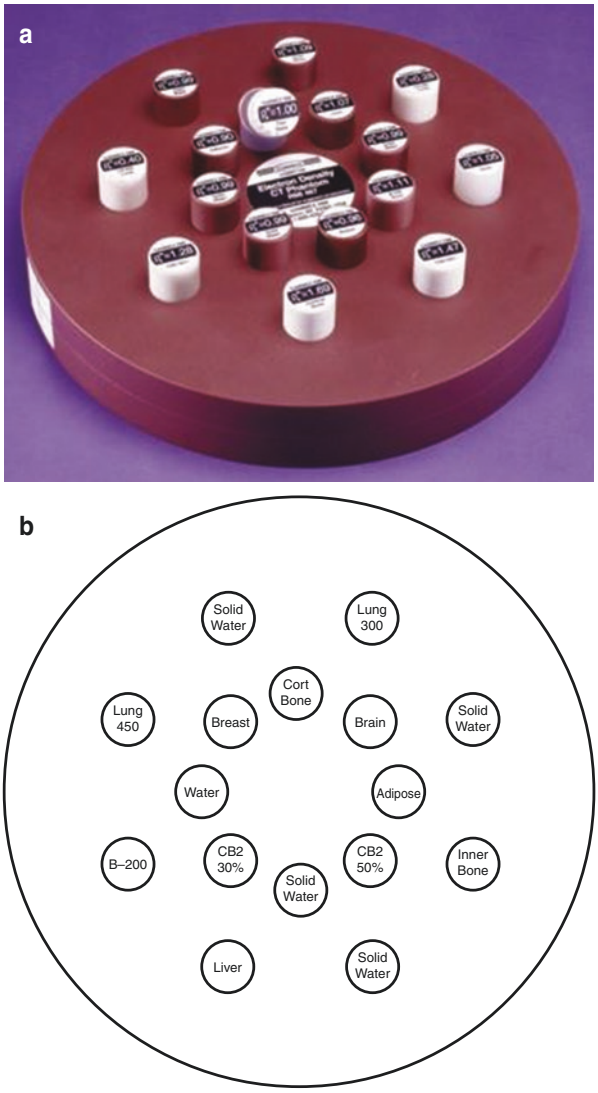

Fig. 3.6 (**a**) Gammex tissue characterization phantom. (**b**) Arrangement of tissue substituting rods (Courtesy of Sun Nuclear)

3.2.1.4 4D CT

- Four-dimensional CT is routinely used to acquire target motion amplitude, allowing moving target treatment planning and active motion mitigation strategies for proton beams:
  - Proton centers may have motion thresholds above which PBS or proton therapy in general is not used.
  - Common thresholds for moving targets treated with PBS are established based on the motion mitigation techniques available and planning techniques (selecting beam direction along the largest component of motion,

smaller spot spacing, use of larger spots) and delivery techniques (optimized delivery sequence, layered/volumetric rescanning); a typical value that is commonly used is 1 cm.

3.2.1.5 DIBH [25, 26]

- Deep inspiration breath-hold (DIBH) has been used to reduce the motion of moving targets and is commonly used in the treatment of breast, lung, mediastinal, and gastrointestinal targets.
- DIBH increases lung volume, can displace normal lung and/or heart away from irradiated regions, and may displace the target volume away from the spinal cord in some cases [27].
- DIBH can significantly reduce heart and lung doses in some cases [28].

3.2.2 Materials and Positioning in the Beam

Like for conventional radiotherapy, patient immobilization materials are adjusted to patient-specific geometry for particle therapy (Fig. 3.7).

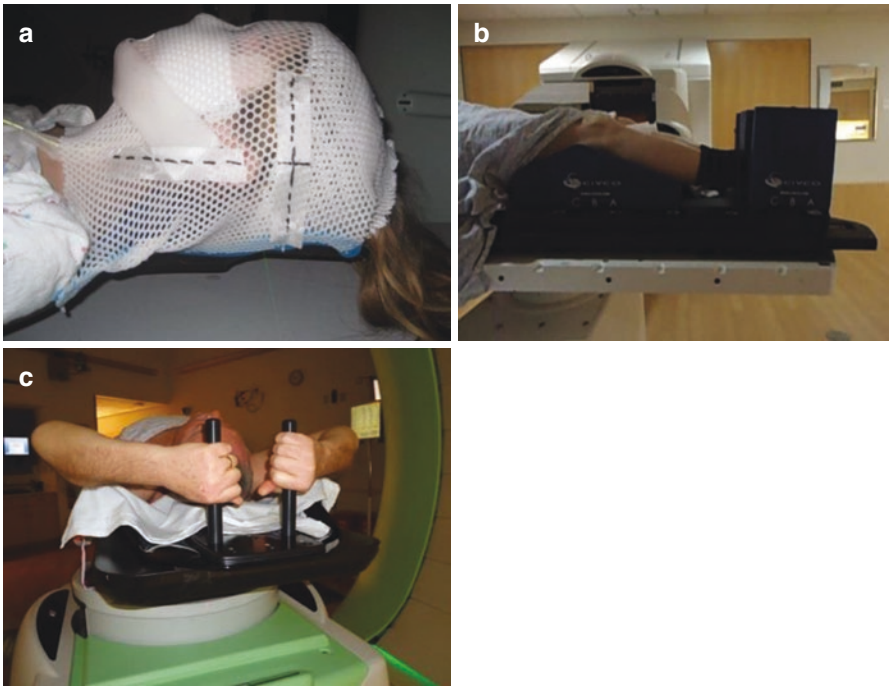

Fig. 3.7 Examples of patient immobilization used at the Hospital of the University of Pennsylvania (**a**–**d**), (**a**) CNS, (**b**) pelvis, (**c**) thorax, and (**d**) shoulder, and Massachusetts General Hospital (**e**, **f**), (**e**) cranial SRS and (**f**) cranial SRS

Fig. 3.7 (continued)

For particle therapy, the following additional principles apply [29]:

- Immobilization devices can be used in contact with skin, as there is no buildup effect for heavy charged particle beams.
- Immobilization devices present in the treatment beam should be minimal and indexed as particle beams are highly sensitive to changes in radiologic depth due to the sharp distal falloff of the Bragg peak.
- Immobilization devices should be radiologically thin in order to minimize the lateral penumbra (due to scattering) and thus preserve dose conformality and lateral sparing of OARs.
- For fixed beam or partial gantry, when the patient rotates with the couch, extra immobilization may be needed to reinforce lateral support.
- Patients have to be positioned in the most comfortable treatment position in order to achieve reproducibility.

3.2.2.1 Treatment Couch

While the attenuation of treatment beam by the couch for X-ray treatments is usually negligible, there is a clinically meaningful shift in range of proton beam for proton treatments [30] (Table 3.3).

Table 3.3 Examples of couch tops currently used for proton therapy

Device	Vendor	WET
Hitachi couch extension QFIX proton	Hitachi Ltd., Japan	1.1 cm
kVue couch QFIX Standard Couch	WFR Aquaplast, Avondale, PA WFR Aquaplast, Avondale, PA	0.55 cm 1 cm

- Determine WET experimentally. This should be done by:
  - Measure proton PDD and range through multiple points in each device.
  - Traditionally with a water-scanning parallel plate chamber:
  - Ensure homogeneity within a given device.
  - Check consistency between devices within a clinic.
  - If measured WET matches calculated value, include full couch top in simulation CT dataset and incorporate couch into calculation. If measured WET does not match calculated value, contour couch top in the treatment plan and override CT numbers to achieve correct.

3.2.2.2 WET

1. Edge effects can be mitigated by:
   - Indexing all immobilization equipment to treatment couch
   - Avoiding treatment beams that traverse couch edges
2. The couch should be designed to be:
   - Free of heterogeneities
   - Base end mounted on robotic positioners with six degrees of freedom
   - Contoured surfaces:
     - Excessive adipose tissue may exhibit widely varying shapes from day to day:
       Posterior neck in H&N treatments [31]
       Pelvis contour in prostate and GYN treatments
     - Variable external contour leads to changes in target depth
     - A customized, contoured couch surface can help present a consistent external contour to the proton beam

3.2.2.3 Range Shifter

- Minimum range for most proton therapy systems is at least $\sim$ 4 g/cm^2 (70 MeV).
- Treatment of superficial lesions requires a range shifter—typically mounted in the head of the machine.
- Range shifters have nonzero scattering power, and so any air gap between range shifter and patient can lead to dramatic increase in spot size [32, 33].
- Place range shifter on or in the couch.

3.2.2.4 Endorectal Balloons

- Reduce interfractional and intrafractional variation of prostate position within the body [34, 35].

- Reduce rectal toxicity by limiting volume of rectal wall within high-dose treatment volume.
- Generally more widely adapted in proton centers because localization of soft tissue target alone does not guarantee adequate target coverage.
- Typically filled with water to avoid gas pockets and heterogeneities along the path of beams.
- May be used for treatment of GYN cancer [36].

3.2.2.5 Collision Detection

In order to avoid delays in treatment, it is important to determine the possibility of patient collision during the treatment planning stage in proton therapy [37]:

- Alpha Cradle, leg abductors, and beanbag used in the thoracic, pelvic, or extremity regions are much less motion limiting.
- Size of devices may limit the choice of beam direction or close proximity of aperture, compensator, or range shifter to the patient.
- The close proximity of these devices is critical to maintain sharp lateral dose falloff for double scattering and to preserve beam spot size for scanned beam.

Current commercial treatment planning systems do not allow automated patient collision detection.

3.2.3 PET/MR Imaging

Besides CT, positron emission tomography (PET) and/or magnetic resonance (MR) imaging studies may have been performed with primarily diagnostic intent, even before the decision to use radiation therapy has been taken. These images are also vital for the planning of the radiation treatment as they give essential information about the anatomic site and extent of disease and the location of nearby uninvolved normal tissues.

3.2.4 Image Registration and Fusion

- There has been a proliferation of medical images through the increased use of functional PET for tumor segmentation, staging, and assessment of treatment response. In addition, MR images are being utilized for accurate tumor and organ delineation due to superior soft tissue contrast. Moreover, patients are being imaged routinely using weekly CBCT and repeated CT scans to monitor anatomical changes as part of adaptive treatment (Fig. 3.8).
- Rigid registration is used in the clinic on a routine basis to fuse daily kV images with DRR and CBCT with planning CT to ensure accurate patient setup (Fig. 3.8).

In addition, rigid registration is utilized to fuse inter- and intra-modality images by overlaying information from diagnostic PET/CT and MRI scans over the planning CT. The fused images are used to delineate tumors and organs at risk for treatment planning purposes (Fig. 3.9).

- Deformable image registration plays an essential role in radiotherapy process for tracking anatomical changes (Fig. 3.10), contour propagation and internal target volume (ITV) generation on 4D CT, and dose accumulation for the purpose of adaptive RT (Sect. 8.9).

3.2.4.1 Uncertainties in Registration

- Deformable image registration is an ill-posed problem, and different solutions may exist which leads to uncertainties. Uncertainties are encountered near

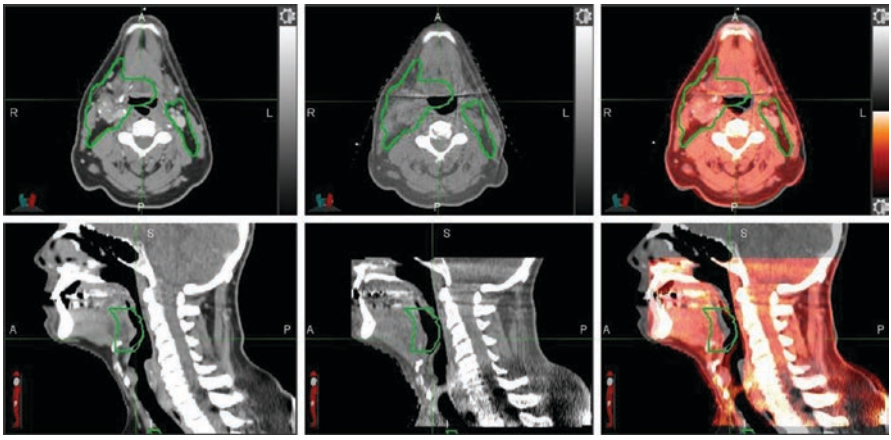

Fig. 3.8 Axial and sagittal views from a planning CT (*left*), CBCT at week 2 (*middle*), and rigidly fused images (*right*) of an example H&N patient. CTV 54 Gy shown in green is overlaid on the CT and CBCT. Notice the tumor shrinkage near the base of tongue which necessitates adaptive planning

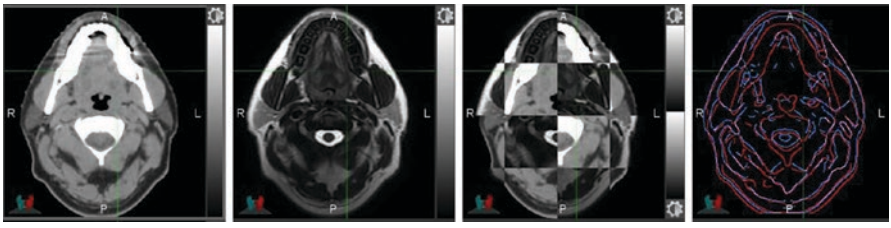

Fig. 3.9 An axial slice of an example H&N patient from a planning CT and follow-up T2-weighted MRI scan. MRI provides better soft tissue contrast compared to CT. Visual inspection of the registration is performed using checkerboard display for image alignment. This process can be facilitated utilizing edges generated from CT and MRI as shown in *blue* and *red*, respectively

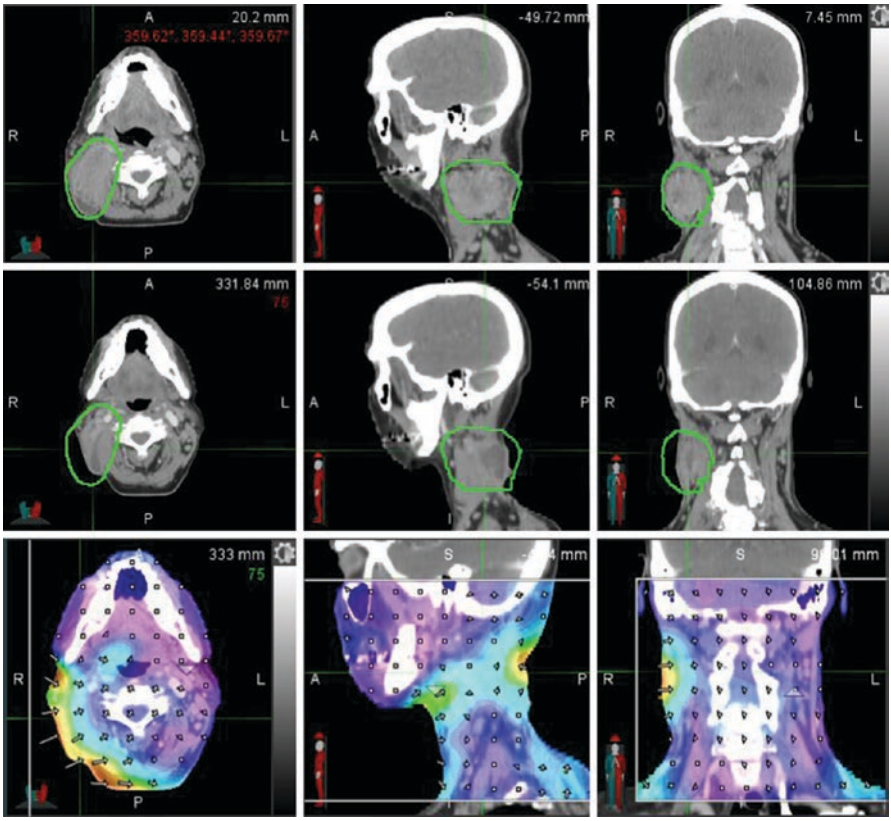

Fig. 3.10 An example H&N patient showing planning CT (*top row*) and a repeated CT (*middle row*). Tumor regression is observed in response to treatment. The deformation grid (*bottom panel*) illustrates regions with large deformation as shown in *red*. Deformation vector fields are also displayed where *large arrows* correspond to large deformations

misaligned edges (bones, tissue-air interface), inside regions of uniform intensity (liver) and of low contrast (lung). These uncertainties are more relevant in proton therapy as compared to photon therapy and must be incorporated into the uncertainty margins of the target (PTV) during the TP process [38].

- Uncertainties in deformable image registration have a direct impact on the dose propagation and accumulation. The spatial uncertainty can lead to large dose errors in the regions of high-dose gradients near the tumor [39]. Larger deformations are usually associated with large registration errors. Consult with physics team to assess the range of dose uncertainty.
- Dice similarity coefficient (DSC; [40]) and Hausdorff distance (HD; [41]) are commonly used metrics to evaluate the quality of the registration based on

physician-drawn contours for segmentation purposes. Several other metrics have been proposed to evaluate the accuracy and underlying uncertainties of the registration such as inverse consistency error (ICE; [42]), transitivity error (TE; [42]), and distance discordance metric (DDM; [43]). However, none of these metrics are considered ground truth, and they need further validation. Several of these metrics rely on the deformation vector field (DVF) of the registration. Guidelines for qualitative and quantitative assessment of deformable registration are emerging but have not been published (AAPM TG 132; [38]). The clinical practices outlined in Table 3.4 are necessary, but not sufficient, to ensure a reasonably accurate registration [38, 44, 45].

- The registration accuracy varies among anatomical sites (H&N, liver, lung, etc.), across image modalities (CT, CBCT, MR), and the choice of registration algorithms (B-spline, Demons, fast free form, etc.). Table 3.5 gives a summary of the absolute registration error reported in literature based on "ground truth" of anatomic landmarks [46–48].
- Overall, the accuracy of deformable registration is on the order of 2–3 voxels. Due to its relevance in proton therapy which is susceptible to range uncertainty, the accuracy of the registration must be investigated for each treatment site for clinical use.

Table 3.4 Guideline for qualitative and quantitative evaluation of deformable image registration

Methodology/metric	Technique	Relevance	Ground truth?
Qualitative			
Color overlay of image difference	Visual	Intensity matching for intra-modality registration	✗
Checkerboard display	Visual	Edge alignment for intra- and inter-modality registration	✗
Quantitative			
Dice similarity coefficient (DSC) Hausdorff distance (HD)	Contour based Contour based	DSC ~ 1 corresponds to better volume overlap Small HD value corresponds to better registration	✗ ✗
Average surface distance (ASD)	Contour based	Small ASD value corresponds to better registration	✗
Anatomic landmarks/ implanted markers	Landmark based	True registration error (TRE)	✓
Jacobian determinant of DVF	Voxel-wise	$J < 0$ corresponds to tissue folding (nonphysical)	✗
		$0 < J < 1$ corresponds to shrinkage (tumor regression)	✗
		$J > 1$ corresponds to expansion (tumor progression)	✗
Curl of the DVF	Voxel-wise	Check presence of swirls (nonphysical deformations)	✗
Physical or digital phantom (InSimQA)	Voxel-wise	End-to-end test	✓

Table 3.5 Range of absolute registration error for different anatomical sites

Modality	Site	Landmarks	Range of mean abs. error	Standard dev.	Max. error
CT/CT [39]	Head and neck	Physical phantom	2.1 mm	2.2 mm	N/A
4D CT [46]	Lung	Bronchial bifurcations	2.0–2.5 mm	2.5 mm	12.0 mm
	Heart and aorta	Calcifications	2.5–5.0 mm	2.5–5.0 mm	6.7 mm
	Liver	Vessel bifurcations	2.5–5.0 mm	2.5 mm	10.0 mm
	Left kidney	Vessel bifurcations	2.5 mm	3.0 mm	3.3 mm
MRI/CT [46]	Liver	Vessel bifurcations	1.1–5.0 mm	2.5 mm	7.0 mm
MRI/MRI [46]	Prostate	Gold seeds	0.4–6.2 mm	0.3–3.4 mm	8.7 mm
CT/CT [47]	Lung	Bronchial branch pts	1.6–4.2 mm1	N/A	15.0 mm
CT/CT [48]	Head and neck	Bone and tissue	2.01–5.16 mm	1.29–2.52 mm	N/A

3.3 Anatomy Modeling, Overrides, CT, Average CT, and MIP

An accurate 3D or 4D model of the patient is established through CT simulation, which is essential for geometric treatment planning. CT images are used to map the patient anatomy to a distribution of proton stopping power ratio.

3.3.1 Artifact Reduction

3.3.1.1 Beam-Hardening Artifacts

- Besides uncertainty of the CT-SPR calibration curve, beam hardening contributes additional uncertainty in SPR values.
- Lower-energy photons have a higher cross section for the photoelectric effect and are absorbed with a higher probability than higher-energy photons. This results in a hardening of the spectrum.
- In all diagnostic scanners, a correction for this effect is applied in the calculation by the scanner software.
- This is only perfect for a standard situation (16 cm cylindrical water phantom) but is incorrect if high-Z materials (e.g., metals) are present.
- Beam hardening makes the calibration curve dependent on patient size [14].

3.3.1.2 Artifact Reduction Algorithms

- Projection completion method [49]
- Iterative artifact reduction methods [50]

3.3.2 Delineation and CT Number Override

- The standard practice to deal with metal CT artifacts is to delineate artifact regions and to reset the CT number of these regions to average soft tissue or bone values measured in similar areas of the body where no artifacts are present [51] (Fig. 3.11).
- The average values may be obtained from artifact-free regions of the same CT dataset.
- High-Z materials which are included in the treatment fields will be contoured and assigned a CT number consistent with the proton stopping power of that material.

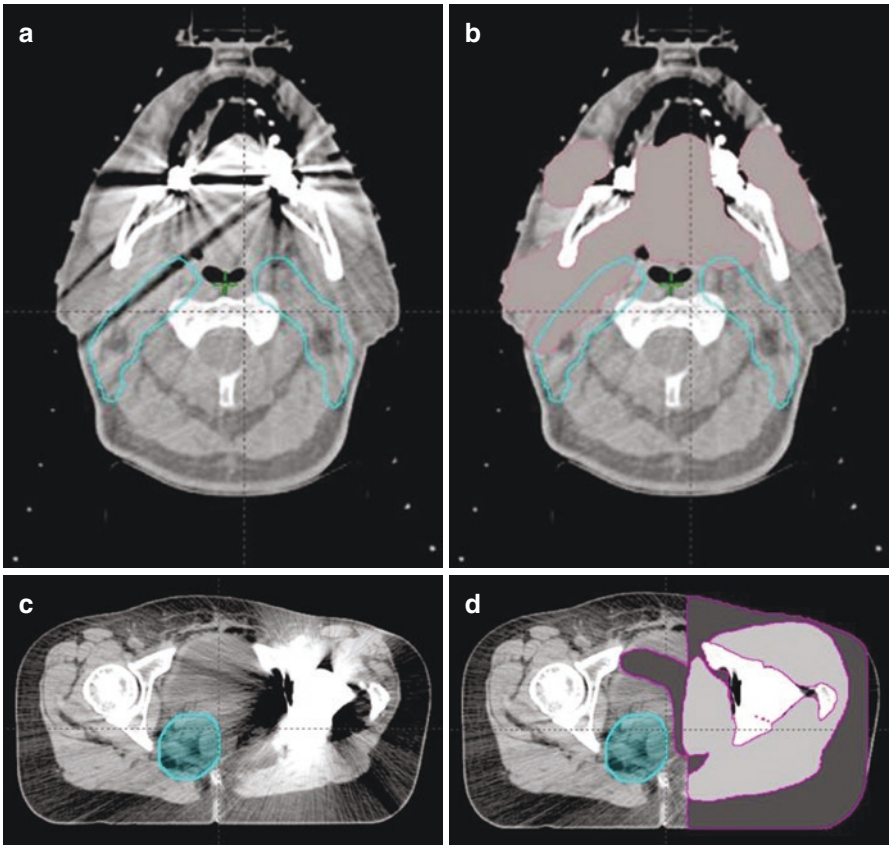

Fig. 3.11 Examples of image artifacts overriding. (**a**) Before overriding, (**b**) after overriding, (**c**) before overriding, (**d**) after overriding

3.4 Anatomy Modeling

1. Barium-doped plastic catheters will be overridden with 0 HU or the CT number of the tissue displaced by the catheter.
2. Metal (small clips and mesh) that does not saturate the CT scanner will not be overridden, although any imaging artifacts resulting from this material will be corrected as described above (sampling similar tissues without artifacts):
   - While this is a time-consuming process, it usually leads to adequate results.
   - Bowel gas is overridden as tissue for dose calculation in order to improve target coverage robustness with respect to daily bowl gas variation.
   - The override could cause the beam to overshoot into neighboring OARs, which can be evaluated by calculating the plan on the same CT without gas overridden (Fig. 3.12).

3.4.1 4D CT [52]

- Average CT—average density values of slices:
  – Better approximation of breathing motion
  – Used for treatment plan dose calculation and display (Fig. 3.13)

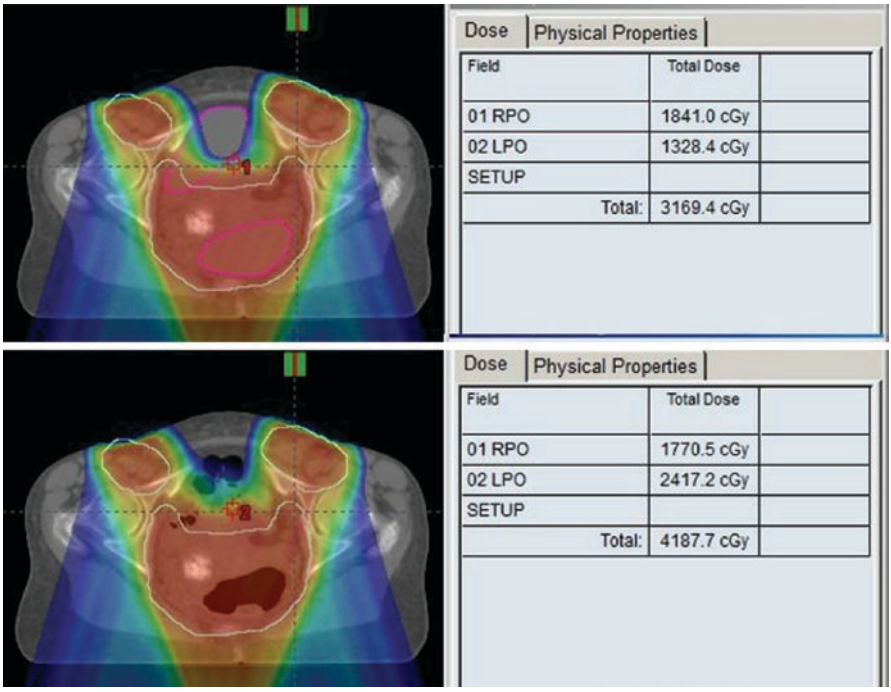

Fig. 3.12 Example of the effect on OAR dose from overshoot. *Top*, dose calculated with bowel gas overridden; *bottom*, dose calculated *without* overridden

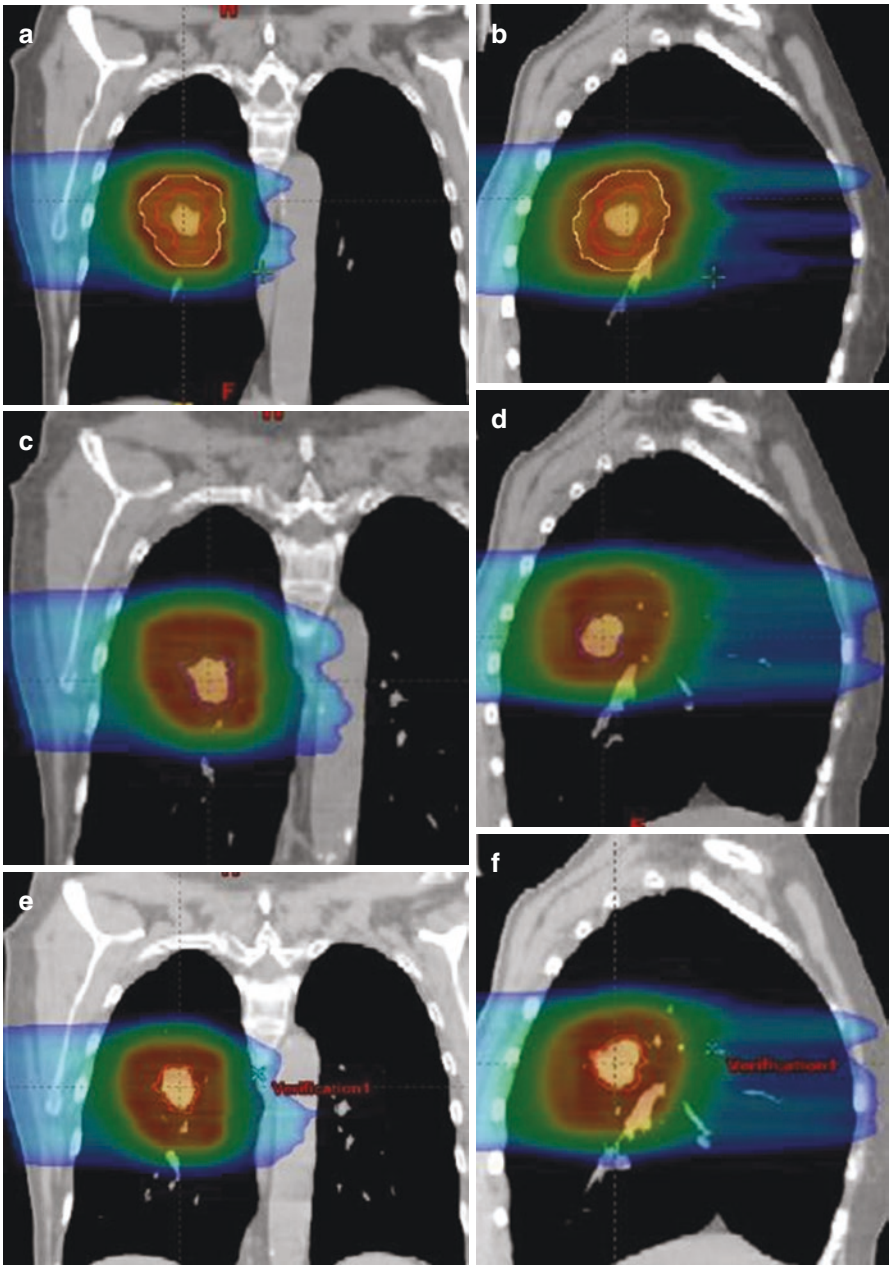

Fig. 3.13 Dose distributions calculated on average CT (**a**, **b**), (**a**) average CT, frontal, and (**b**) average CT, sagittal; end-inhalation CT (**c**, **d**), (**c**) end of inhalation, frontal, and (**d**) end of inhalation, sagittal; and end-exhalation CT (**e**, **f**) with identical beamline, (**e**) end of exhalation, frontal, and (**f**) end of exhalation, sagittal

  - May need CT number override of IGTV with a conservative estimation of densities in order to ensure tumor coverage. However, this approach may compromise OAR sparing
- Any single phase:
  - Extreme phases (inhale and exhale) used to evaluate coverage by forward calculation using planned beamline (Figs. 3.13 and 3.14)
- MIP image—maximum intensity projection; maximum density value of slices:
  - Conservative since maximum density is provided
  - Should guarantee dose coverage of distal target
  - Lose coverage in proximal target region
  - Employed for targets located in the lung
- End-expiration phase (e.g., in Fig. 3.13):
  - Provides better stability and reproducibility [53]

4D CT-based planning is described in further detail in Sect. 5.

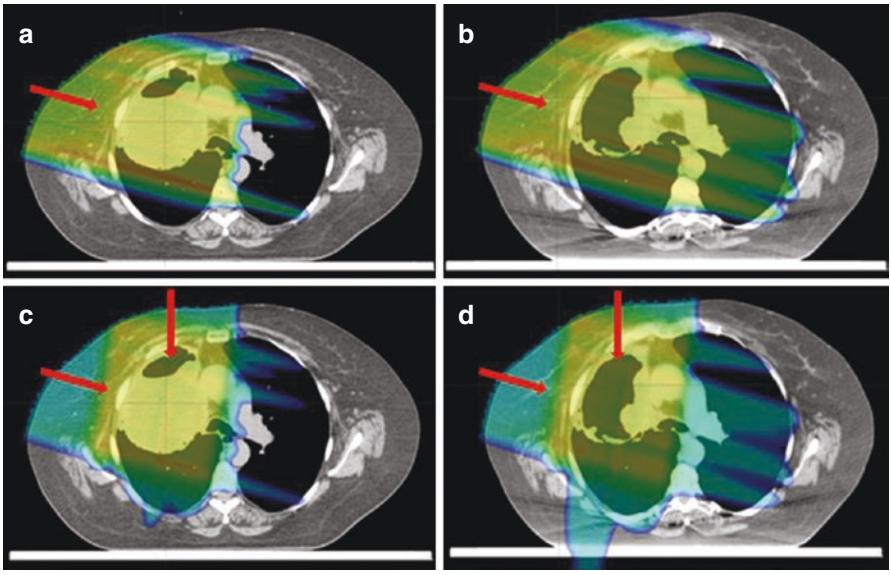

Fig. 3.14 The effect of lung tumor shrinkage on proton dose distribution. The second CT scan was taken at 3 weeks into treatment course. (**a**) shows a single RAO field from the nominal treatment plan; and (**b**) shows the effect of tumor shrinkage on the RAO field. (**c**) shows the complete two-field nominal plan; and (**d**) shows the effect of tumor shrinkage on the two-field plan

3.5 Beam Design Characteristics

3.5.1 Passive Scattering

With passive scattering (PS) beam delivery, the beam is broadened as it passes through the delivery nozzle and spreads uniformly over a large area (Chap. 2). A major difference between proton beams and photon beams is that individual proton beams may be designed to cover the entire target volume with a uniform dose distribution, characterized by the proton range, field size, and modulation width of the spread-out Bragg peak (SOBP). Field shaping is achieved by customizing the field aperture, proton beamline, and range compensator designs to ensure conformal coverage of the CTV with appropriate lateral margins and beam-specific distal and proximal margins to account for proton range uncertainties.

3.5.1.1 Beam Design Characteristics

- Field aperture: Typically manufactured from brass plates; however, some facilities use Cerrobend blocks or multi-leaf collimators (MLC). Designed to conform dose to the CTV in the beam's eye view (BEV), including margin for internal motion of target (IM), margin for setup uncertainty (SM), and a dosimetric margin to account for the physical and geometrical lateral penumbra, typically defined from the field edge (50% isodose level) to the prescription isodose, ($P_{50\%,\,Rx\%}$).

Aperture lateral margin (LM) (Fig. 3.16b) from the CTV at the isocenteric plane is given by

$$LM = IM + SM + P_{50\%,\,Rx\%}.$$

The physical dimensions of the aperture will be a function of nozzle position relative to the isocenter.

- Distal and proximal margins: Distal margins (DM) and proximal margins (PM) are defined from the CTV (Fig. 3.15) and are realized by appropriate combination of beam range and SOBP width. Both DM and PM are range dependent, with 3.5% of the range [4–6] plus 1 mm used typically.

Required range (R) is given by

$$R = R_d + DM = 1.035R_d + 1\ \text{mm},$$

where R_d is the maximum range needed to cover the distal edge of the CTV without margin (Fig. 3.15). R_d is established by initial calculation of the water-equivalent thickness (WET) along the beam path to the most distal point of the CTV.

The required SOBP width is given by

$$SOBP = R_d - R_p + PM + DM = 1.035R_d - 0.965R_p + 1.0\ \text{mm},$$

where R_p is the minimum range needed to cover the proximal edge of the CTV without margin (Fig. 3.15).

The beam-specific distal and proximal margins give rise to the concept of the beam-specific PTV (bsPTV) [54], defined by the prescription isodose curve of each individual beam (Fig. 3.16).

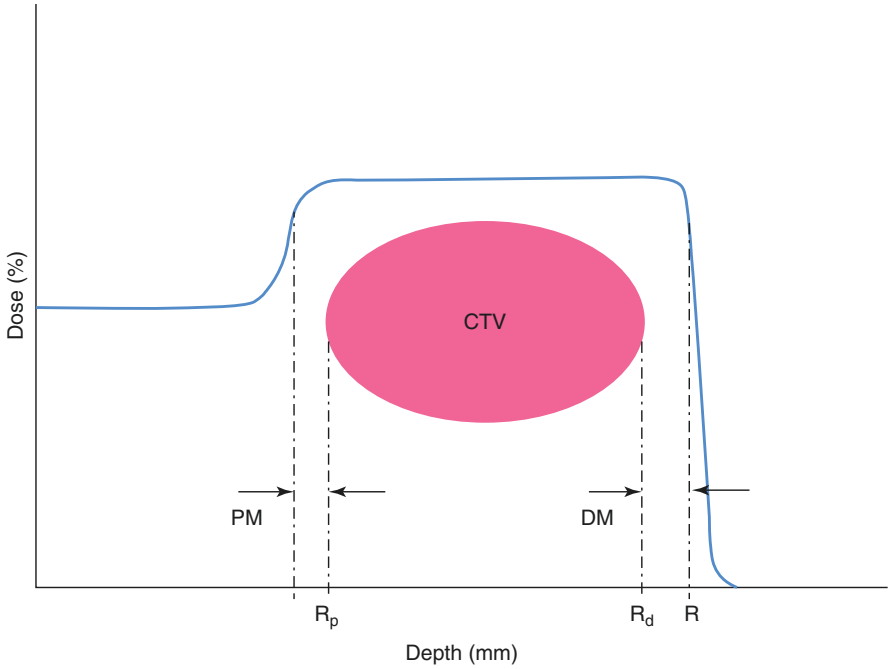

Fig. 3.15 SOBP covering CTV with distal margin, DM, and proximal margin, PM, where R is range, R_d is maximum range needed to cover CTV distal edge, and R_p is minimum range needed to cover proximal edge of CTV

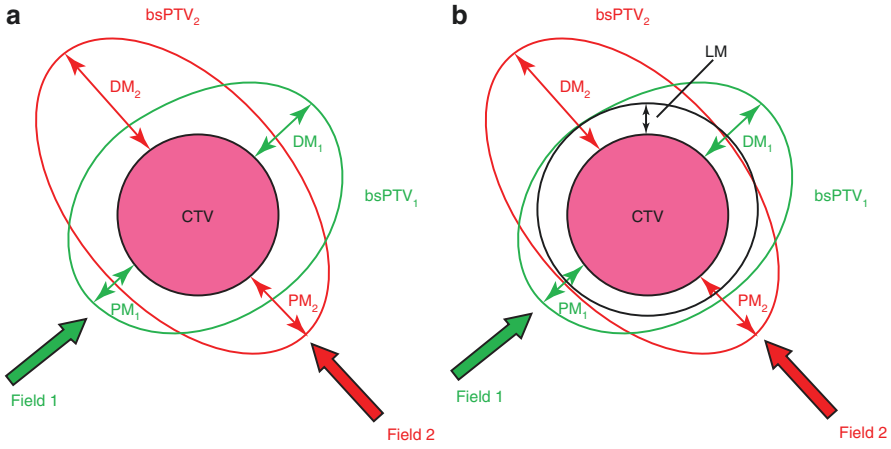

Fig. 3.16 (**a**) Beam-specific distal margins (DM) and proximal margins (PM) giving rise to a beam-specific PTV (bsPTV) for each field. (**b**) Lateral margins (LM) for both fields, similar in concept to the photon PTV

- Range compensator: Typically manufactured from PMMA, although some facilities use wax. Designed to conform the distal end of the beam to the distal edge of the CTV with DM and account for heterogeneities along the beam path, by pulling back the distal end of the beam. This is achieved with the compensator designed to be of varying thicknesses along each ray line across the BEV. It should be noted that the calculated range, R, includes the minimum WET of the compensator.

Smearing is applied to the design of the compensator to account for lateral setup uncertainty and internal motion of anatomy. Once the ideal thickness of the compensator at each point is calculated with a ray-tracing algorithm, circles of a specific smearing radius (SR) are superimposed over the calculation grid, centered at each point. The compensator thickness within each circle is reduced to the minimum at any point within the circle.

The SR is given by

$$\mathrm{SR} = \sqrt{(\mathrm{IM} + \mathrm{SM})^2 + (0.03R)^2},$$

where the first term accounts for internal motion and setup uncertainty and the second term accounts for proton lateral scatter [4, 55, 56].

Smearing has the effect of making the distal dose less conformal on a static treatment plan but ensures distal coverage with positional uncertainty (Fig. 3.17).

While the range compensator conforms the dose to the distal edge of the target, a major limitation of PS proton beams is the inability to conform the dose to proximal side of the target. This is because the beam is modulated to a fixed SOBP width across the entire field (Fig. 3.18).

Summary of PS beam parameters is given in Table 3.6.

3.5.1.2 Treatment Planning

Despite the fact that a single proton beam can cover the target volume, it is typical to use multiple beam angles to mitigate the effect of proton-specific uncertainties (Table 3.1). This is particularly useful if an organ at risk (OAR) lay just distal to the target to spare that OAR from end-of-range effects such as higher RBE related to increased LET [12]. Multiple beam angles also help to reduce skin dose [57], given that passively scattered proton beams do not display effective skin sparing.

- Beam direction: The choice of beam direction is extremely important in designing a robust proton treatment plan. As the absolute uncertainty in proton range increases as a function of path length, choosing beams that travel the shortest distance to the target reduces both the DM and PM and reduces the integral dose. However, beam directions are often chosen so as to protect OAR that lay distal to the target from end-of-range effects [12]. In such circumstances, a beam direction may be chosen such that its lateral edge, rather than its distal edge, is used to block an OAR. Furthermore, as protons are sensitive to the radiological path

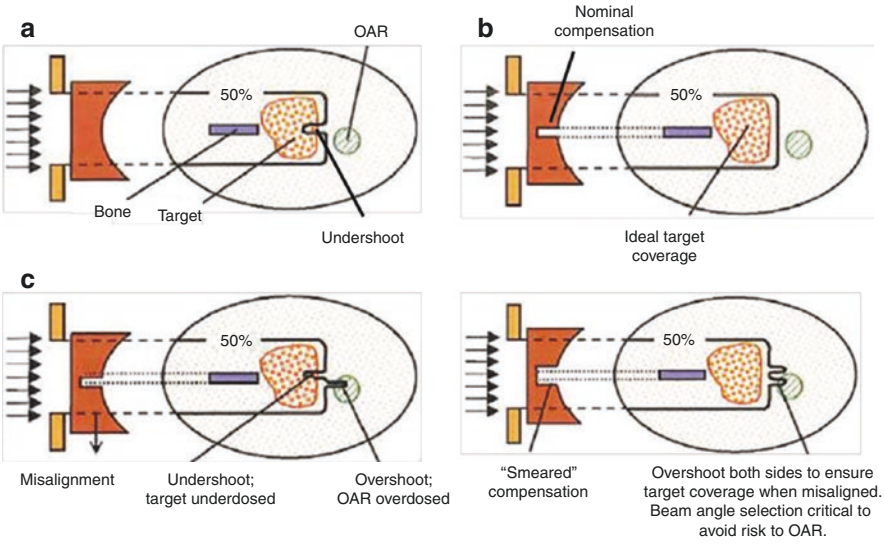

Fig. 3.17 The effect of the range compensator with and without smearing: (**a**) no compensation; (**b**) nominal compensation, without smearing; (**c**) effect of misalignment without smearing; (**d**) compensation with smearing

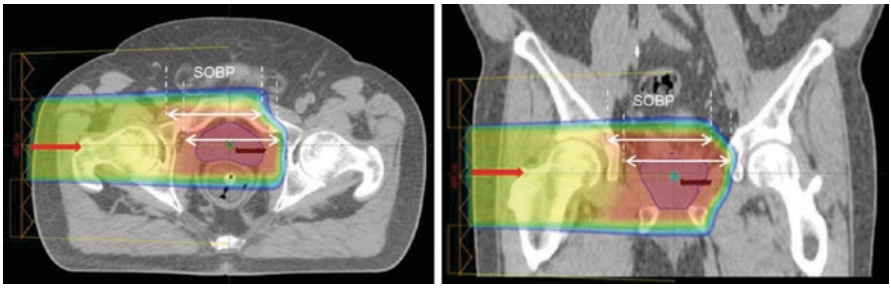

Fig. 3.18 Single right lateral field to the prostate. The distal end of the SOBP conforms to the target shape because of the compensator; however, the proximal side of the SOBP is not conformal because of the fixed SOBP width

along which they travel, choosing beam angles that avoid variations in the anatomy caused by, for example, bladder filling, bowel gas variation, stomach filling, respiratory motion, or other such processes is preferable. If at all possible, directions with abrupt changes in proton stopping power (highly heterogeneous) should be avoided. Directions, for example, that are oblique to the patient surface, or that travel through high-density materials such as titanium rods, or that travel through the edge of patient immobilization devices or the couch edge, are all highly susceptible to range uncertainty and therefore have to be avoided (Table 3.1).

Table 3.6 Formulae for calculating passive scattering beam-specific parameters

Beam-specific parameter	Formulae
Aperture lateral margin from CTV	$\mathrm{IM}+\mathrm{SM}+P_{50\%,\mathrm{Rx}\%}$
Range margins	$1.035R_{\mathrm{d}}+1.0$ mm
SOBP width	$1.035R_{\mathrm{d}}-0.965R_{\mathrm{p}}+1.0$ mm
Smearing radius	$\sqrt{(\mathrm{IM}+\mathrm{SM})^2+(0.03R)^2}$

R range, R_{d} maximum range needed to cover CTV distal edge, R_{p} minimum range needed to cover proximal edge of CTV, SM setup uncertainty, IM internal margin, $P_{50\%,\mathrm{Rx}\%}$ penumbra width from field edge to prescription isodose

- 4D CT-based planning: Treatment planning of thoracic and abdominal targets with significant respiratory motion is typically based on 4D CT. 4D CT data are acquired and binned into 3D datasets representing different phases of the respiratory cycle. Maximum-intensity projection (MIP) and intensity-weighted average projection (average CT) datasets are generated. The envelope of motion of the GTV—the internal GTV (iGTV)—is contoured either on the MIP (when the target has large contrast in CT, e.g., in the lung) or from the union of GTV contours from all phases. The iGTV contour is copied onto either the average CT or a mid-ventilation dataset on which the nominal plan is calculated. The iGTV is uniformly expanded to be the iCTV to encompass microscopic clinical disease. The CT numbers are overridden according to tumor density throughout the iGTV in order to provide a conservative estimate of radiological path lengths for all positions of the GTV, ensuring distal coverage of the target throughout the respiratory cycle (Fig. 3.19). This results in proton-beam overshoot across much of the field; and so distal OARs need to be considered when choosing beam direction. Planning to the iCTV is done using the margins described above. IM is set to zero in the calculation of LM and SR as the internal motion has been accounted for. Nominal treatment plan may be reviewed on the end-inhalation and end-exhalation phases to verify target coverage in these extremes (Fig. 3.20).
- Abutting fields: For large or elongated volumes, two or more adjacent fields may need to be used from any given beam direction. This typically requires multiple isocenters and dosimetric matching of field penumbrae at depth. The classic example of this is craniospinal irradiation (CSI) with PS proton beams (Fig. 3.21) [58]. Due to the sharp lateral falloff of dose for PS fields shaped with an aperture, numerous sets of match fields are planned with the match line displaced 1 cm or so to reduce uncertainty at match line locations. Each set of fields is only delivered for a proportion of the total number of fractions. This is labor intensive and expensive as new apertures are required for each set of fields. By comparison, pencil-beam scanning (PBS) techniques for CSI can use intensity modulation to improve matching field robustness [59, 60].
- Patch fields: Patch-field planning may be used when a target wraps around an OAR in very close proximity. To avoid directing a beam toward the OAR, a "shoot-through" beam is used to cover part of the target, while a "patch" field,

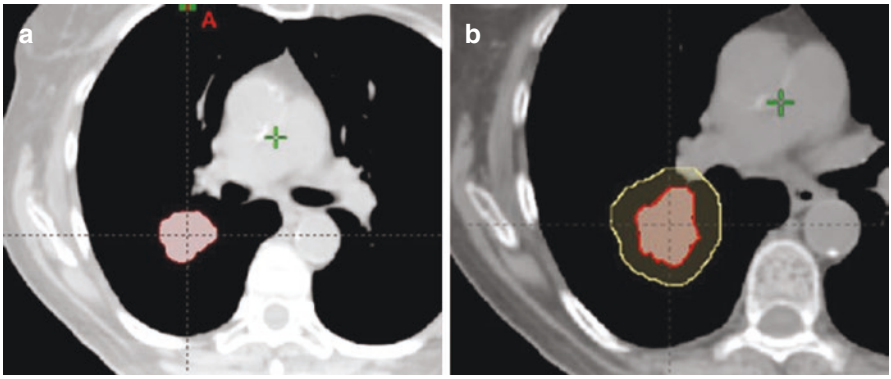

Fig. 3.19 (**a**) iGTV contour on average CT (or mid-ventilation) dataset with CT numbers overridden to provide a conservative estimate of radiological path lengths throughout the respiratory cycle; (**b**) uniform expansion to the iCTV

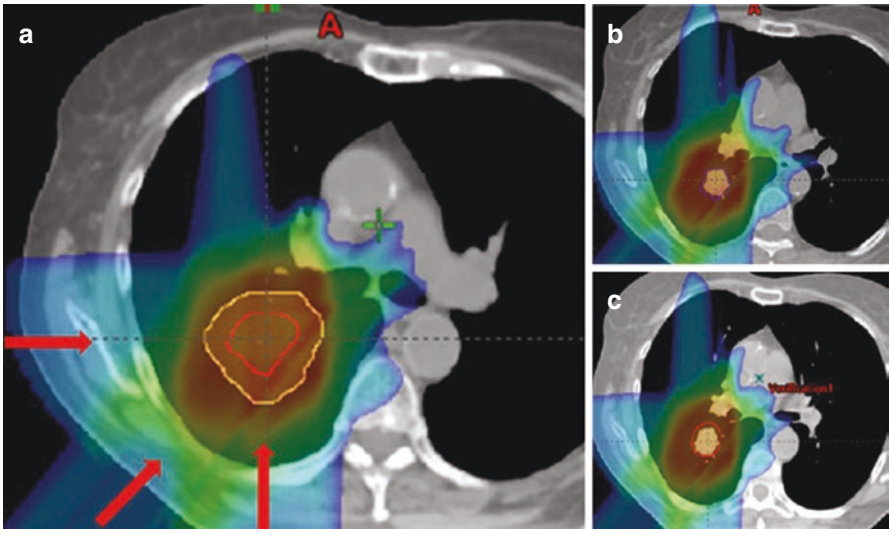

Fig. 3.20 (**a**) Nominal plan on average CT (or mid-ventilation) dataset, with plan evaluated on (**b**) end-inspiration phase and (**c**) end-expiration phase

covering the remaining part of the target, is designed such that its distal edge matches the lateral edge of the "shoot-through" beam [61]. Both beams block the OAR with their lateral edges (Fig. 3.22). The distal penumbra of the "patch" field is typically sharper than the lateral penumbra of the "shoot-through" field. As a consequence, matching the 50% isodose lines of these beams at the patch line produces hot and cold spots. As the patch line is typically within the CTV, the match is planned erring slightly toward being hot rather than cold. To mitigate the overall effect, the beam direction of the "shoot-through" and "patch" are reversed on alternating fractions, thus changing the location of the patch line.

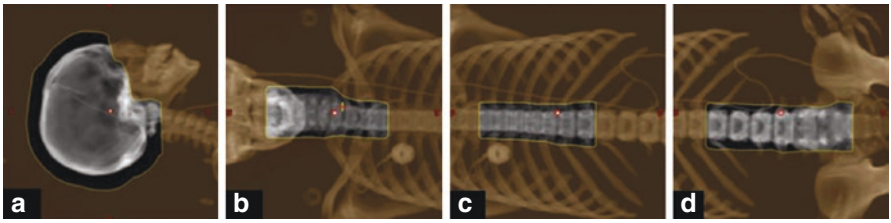

Fig. 3.21 Field-defining apertures for (**a**) cranial, (**b**) upper spine, (**c**) mid-spinal, and (**d**) lower spine fields matched for total craniospinal irradiation (CSI). Four isocenters are used in this example

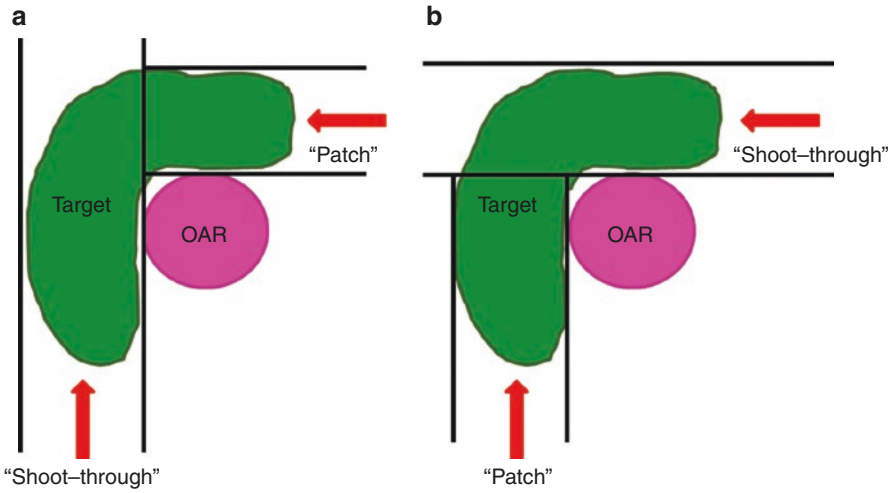

Fig. 3.22 Patch-field setup to cover the target while sparing the OAR. (**a**) shows "shoot-through" and "patch" field directions chosen to avoid range uncertainty risk to the OAR; and (**b**) shows beam arrangement used on alternating days to mitigate dose heterogeneity within the target at the patch line

As each component of the patch field is designed to cover only a portion of the target, they are inherently less robust than other PS field designs. It is therefore recommended that robustness analysis be performed to evaluate the dosimetric consequences of uncertainties.

3.5.2 Pencil-Beam Scanning

3.5.2.1 Proton Pencil-Beam Features

Any radiation beam has two features:

- Geometry: its orientation and placement with respect to the patient and target
- Dosimetry: its ability to deposit dose within the patient

The geometric approach of a radiation beam correlates with its dosimetric abilities. That is, for example, a single photon beam has little or no dosimetric control along the penetration axis of the field. This limitation is mitigated by adding many other photon fields to achieve conformal abilities. A single proton beam, however, has the ability to achieve full conformality and less or sometimes even no additional fields are needed. Thus:

- Geometric placement of proton fields can be used to greater advantage, compared to photon fields, to achieve normal tissue sparing. That is, proton field placement can completely avoid normal structures if desired.
- Geometric placement of proton fields can enhance the penumbral falloff between target and OAR. Since fewer fields are needed, the field-intrinsic penumbra can be preserved. In contrast, a complex photon field arrangement (such as IMRT) inherently creates a washout of the penumbra as a consequence of the continuous overlap of fields. In practice, IMRT penumbra can only be preserved along a narrow surface parallel to the rotation axis as in rectal wall sparing in prostate treatment (see Fig. 3.23).
- Geometric placement for PBS beams pragmatically aims to achieve the least healthy tissue between the skin and the target and achieves maximal OAR avoidance.

The dosimetric ability of a proton pencil-beam field is defined by numerous spots with the ability to modulate the dose within each spot contained in a three-dimensional sub-volume of the target:

- A spot is a "narrow" single-energy proton pencil beam deflected magnetically to a location (x, y) in the isocentric plane with a penetration proportional to the energy and of a particular intensity defined by the number of protons in the pencil beam. The spot location is typically indicated with the radiological depth of its 90% range, R_{90}.
- The set of all beam spots is, initially, chosen such that the spot locations form a regular grid (rectangular or hexagonal) at a constant energy (range) (see Fig. 3.24):
  - Spots placed at a constant energy are referred to as a spot "layer."
  - The spot grid spacing, typically, is proportional to the spot size σ in air. This overpopulates the spot layer as it excludes the effect of inpatient scatter which increases the spot size to $\sqrt{\sigma^2 + 0.03R^2}$.
  - Multiple layers are stacked across the depth of the target to cover the target. Typical layer spacing is 5–8 mm.
  - Margins in proximal and distal depths are used to allow for range uncertainties and proximal and distal dose equilibrium.
  - Lateral margins (>3σ and see above on the effect of inpatient scatter) are used in each layer to achieve lateral dose equilibrium.
  - For a 100 mm cube, the set of spots could be as many as 10,000 for a small spot (σ ~ 5 mm) given a brute force geometric spot placement algorithm as suggested above.

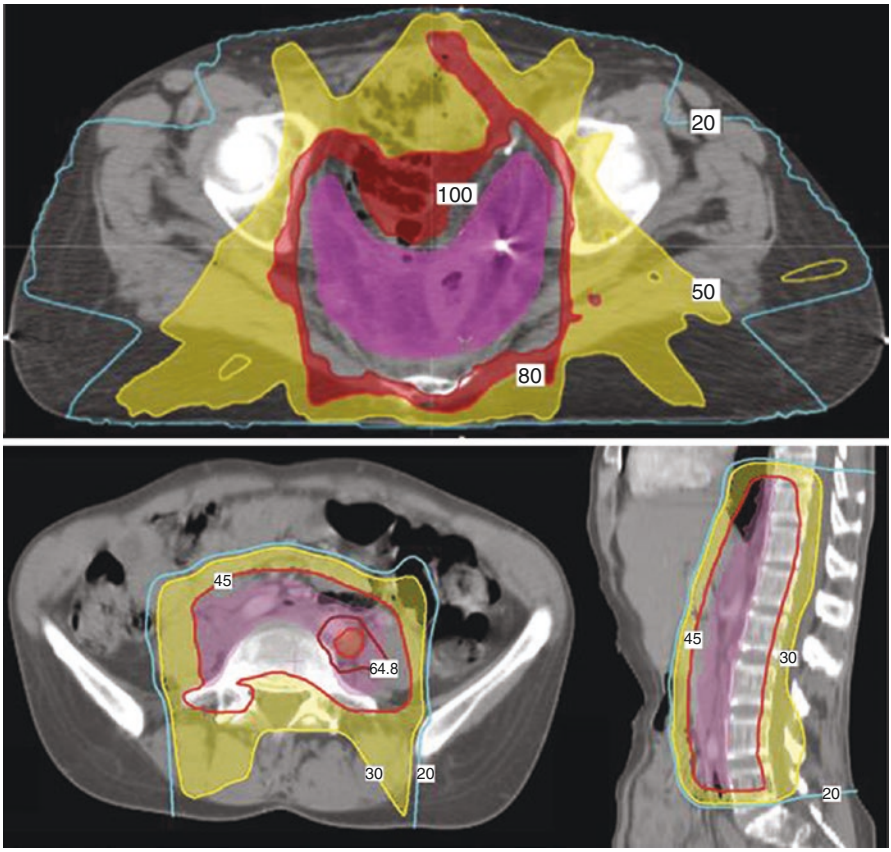

Fig. 3.23 Patient treated for endometrial cancer. The conformality of a single proton field, as in the lower panel, exceeds that of, for example, the IMRT fields shown in the upper panel. The IMRT treatment has an unavoidable dose path throughout the abdomen. Note that the IMRT is in relative dose, while the PBS plan is in absolute dose; 100% equals 45 Gy(RBE) (Image courtesy of Dr. A. Russell and J. A. Adams, Massachusetts General Hospital)

- Spot placement is per beam and ignores (as currently implemented) the spot placement in another beam. The overall consequence of current spot placement algorithms is that there are too many spots in the total set of all beams.

The spot intensities, specified in charge (number of protons) or monitor units, of a set of beams, where a minimum set includes the beams delivered in a treatment fraction, are determined by the optimization algorithm. The spot placement algorithm and spot size affect the spot intensities because:

- The fraction dose to the target volume determines (to the first order) the total number of protons that are required. A rule of thumb is that 1 Gp (giga-protons) is required to deliver 1 cGy(RBE) to 1000 cc. Thus, 2 Gy(RBE) to a liter requires about 200 Gp. Table 3.7 illustrates some consequences of delivery.

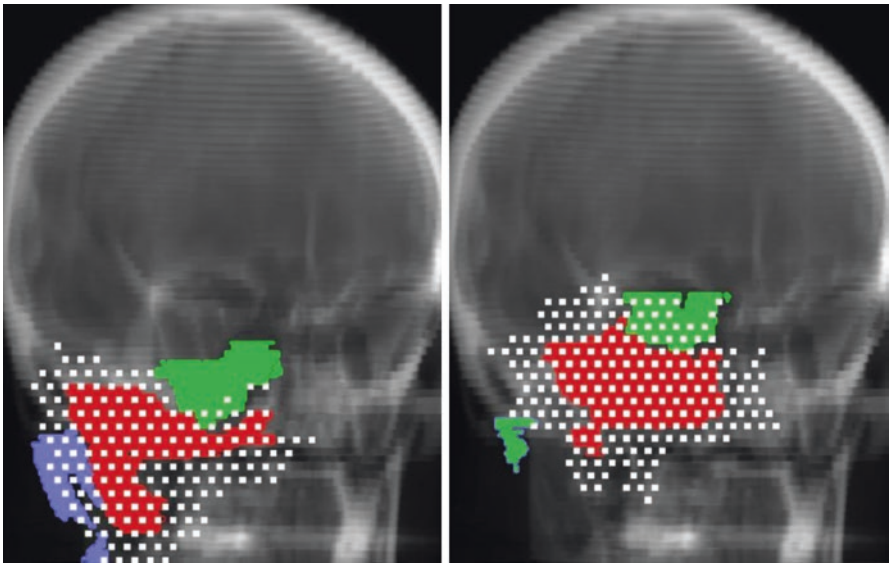

Fig. 3.24 Two spot layers (at different energies). The spot terminal points (i.e., at the radiological depth equal to R_{90}) intersect the patient at different positions as is evident from the volume (target, red; brainstem, green; etc.) intersections. The intersection surface is not a plane (per se) but a surface at constant water-equivalent (in terms of proton stopping power) depth in patient

Table 3.7 Some rule-of-thumb considerations in spot charge and delivery

Desired treatment time	60 s		
Total number of protons	2.00×10^{11}		
Number of layers	15		
Total number of spots	10,000		
Layer switching time/s	2	1	0.005
Spot rate/s	333	222	167
Maximum number of protons per layer	1.40×10^{11}		
Maximum number of protons per spot	2.10×10^{8}		
Maximum current/nA	11	7	6

A desired irradiation of 1 L cube to 2 Gy(RBE) requires 200 Gp (Gp: 10^9 protons). We wish to treat in 60 s. The delivery uses 15 layers with about 10,000 spots (implying a spot size $\sigma \sim 4$ mm). If the layer switching time is 2, 1, or 0.005 s, spots need to be delivered at the rate indicated. Of note, spot rate is primarily limited by the ability to change the magnetic field. The maximum number of protons per layer and spot is approximated by assuming the deepest, distal layer delivers 70% of the total charge. This results in the maximum currents indicated in the bottom row

- A typical charge density across the field is on the order of 1,000,000 protons per mm^2. Much higher local densities are common. It should be obvious, however, that larger spots will have higher mean charges. Thus, a spot twice as large as another spot will have four times the mean charge. The number of protons is distributed over the spots: the more spots, the lower the mean charge of a spot.

- The accelerator typically has a lower limit on the possible spot intensity. If there are too many spots, there may be many spots that have an intensity below this limit.
- All these effects may affect the plan quality in terms of optimization efficiency and quality and in terms of treatment delivery efficiency.

3.5.2.2 Beam Set and Fractions

Proton fractions can readily alternate different combinations of beams, or fraction beam sets, within a particular treatment phase. For example, of a total of five individual beams in a phase, three sets may be defined as (1, 3, 5), (2, 5), and (4, 5). The set combinations may be chosen to alternate healthy dose areas or even be based on practical considerations such as effects on overall treatment time for a fraction. Such beam rotations are not used in IMRT treatments and, as a consequence, are not well established in general clinical practice.

Each beam set must deliver the desired fraction dose. Thus, beam 5 in the above example really has three different dosimetric representations, one for each set. Beam 5 simply refers to its geometric features but its dosimetric features depend on its fellow members. Each beam is thus defined by its geometry (say 5) and its dosimetric state, i.e., beam 5 in fraction 1 or beam 5 in fraction 2.

The use of different beam sets over a phase requires an optimizer that can consider the membership of a beam within the fraction while considering the objectives of the whole course. In the asteroid system (.decimal, Sanford, FL), the user can define:

- Course constraints, e.g., maximum dose to the brainstem less than 54 Gy(RBE), minimum dose to the CTV is 52 Gy(RBE), and so on.
- Course objectives, e.g., try to minimize the brainstem mean dose, try to maximize the minimum dose to the CTV.
- Fraction constraints, e.g., in the five fractions for this beam set, the maximum dose to the brainstem is 10 Gy(RBE).

Table 3.8 shows a fraction group subdivision for a simultaneous optimization for a chordoma treatment. Figure 3.25 shows the dosimetry for the GTV fraction group, obtained while simultaneously optimizing all fraction groups, and the total dosimetry of all fraction groups.

3.5.2.3 Field Matching and Patching

For SOBP fields in PS (see previous section on PS; Sect. 5.1):

- Matching requires two to three feathers to avoid hot or cold spots possible with the sharp SOBP penumbra.
- Patching requires alternate through/patch combination due to the range uncertainty. In practice, a single through/patch combination should not be used for more than five fractions. For PBS fields:

1. Matching is greatly simplified by specifying an overlap volume left/right of the match line and allowing the optimizer to produce a gradient in the region (see Fig. 3.26).

Table 3.8 Three fraction groups to CTV, CTV II, and GTV, each with fraction group constraints and beam allocations. The multiple fractions and constraints are optimized as a single problem

Fraction groups		Number of fractions
1 CTV	Type: IMPT Target: CTV + 5 mm Total dose: 26 Gy(RBE) Constraint: CTV + 3 mm minimum 24 Gy(RBE) beams: R35A CTV, L50P CTV	13
2 CTV II	Type: IMPT Target: CTV + 5 mm Total dose: 24 Gy(RBE) Constraint: CTV + 3 mm minimum 22 Gy(RBE) beams: R50P CTV, L25A CTV	12
3 GTV	Type: IMPT Target: GTV Total dose: 28 Gy(RBE) Constraint: GTV minimum mean 28 Gy(RBE) beams: L70P GTVp3, R50P GTVp3	14

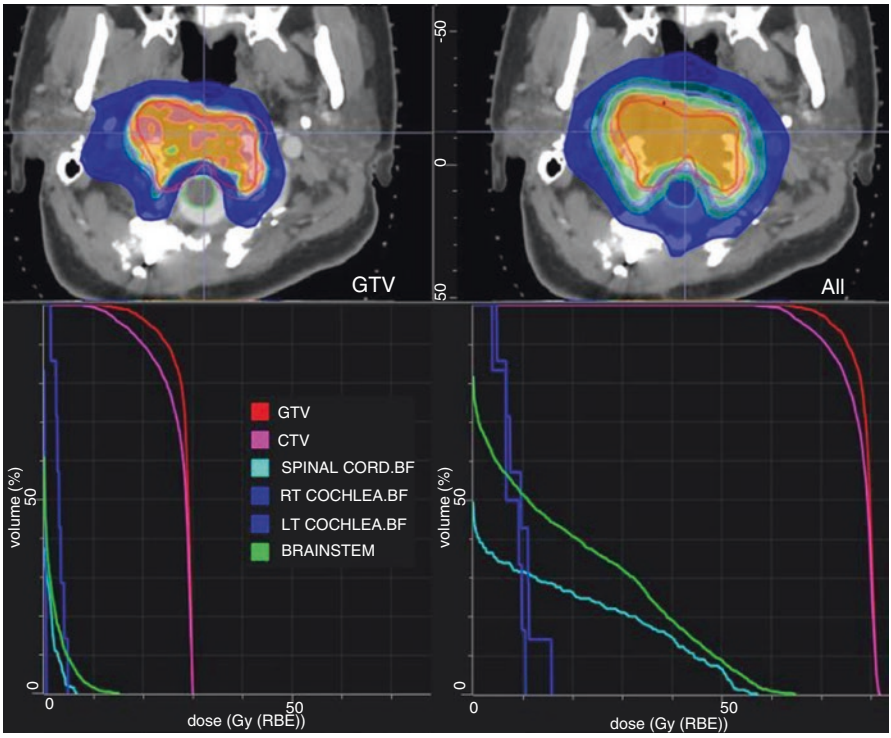

Fig. 3.25 Dosimetry for GTV fraction group and total dosimetry (see Table 3.8). Notice that for the GTV fraction group, the constraint is specified as a minimum mean dose of 28 Gy(RBE)

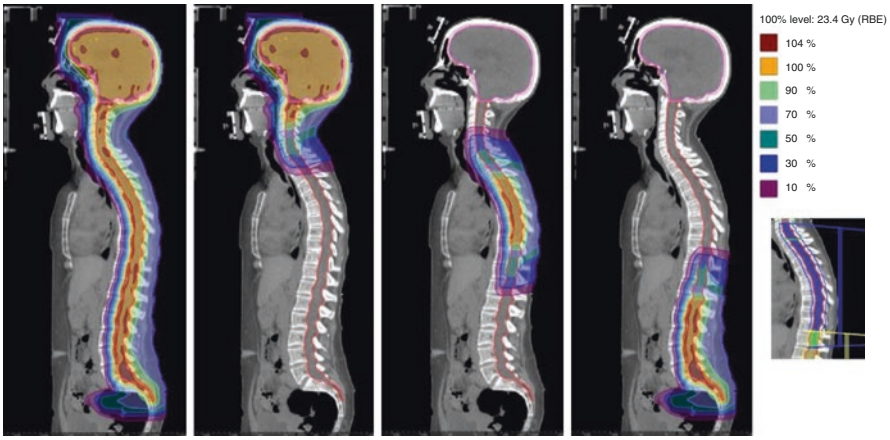

Fig. 3.26 Medulloblastoma patient treated with two cranial fields (to ensure lens sparing) and two posterior fields. Two overlap regions, in the cervical spine and lower thorax, ensure a smooth and long gradient that ensures dose continuation with ±3 mm setup uncertainty. The inset (*right*) shows the overlap region between the thoracic (*blue*) and lumbar fields (*yellow*)

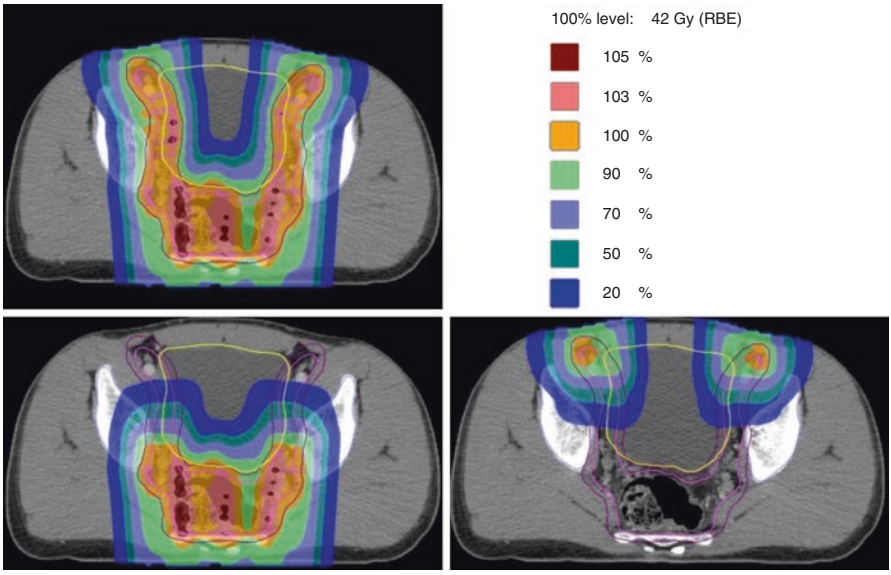

Fig. 3.27 Rectal cancer patient, composite dose top left. Anterior and posterior field patches along the distal edges are allowed to range out over an overlap volume (bottom left/right). Note that the spot size in this example is large which causes the size of the penumbral lateral falloff

2. Patching is obviated as fields are allowed to range out into the each other. This, of course, is subject to robustness considerations (see Fig. 3.27).
   - This does not necessarily imply IMPT fields. SFUD fields can overlap to a lesser extent or otherwise achieve smooth gradients.

3.6 Treatment Plan Design and Site Considerations

3.6.1 Site Considerations

- The effect of treatment site specifics influences the approach and quality of proton fields.
- Range uncertainties and increased LET (ionization density per unit length) at the end of range demand that proton fields cannot range out into a critical structure. Instead, penumbral separation between target and critical structure must be achieved by the lateral edge:
  - Of note, the distal penumbra is typically twice as sharp compared to the lateral penumbra in SOBP fields that use a range compensator. Nevertheless, the distal penumbra should not be used for separation between target and OARs.
  - The distal penumbra in a PBS field is essentially equivalent to the lateral penumbra because the distal penumbra in such a field is comprised of multiple, near arbitrarily positioned, spots.
- Motion effects are particularly troublesome as the motion periodicity requires a consideration of the dose perturbation at every time point:
  - 4D CT can accurately establish the periodicity of the patient's anatomy.
  - In principle, a plan can be designed that simultaneously meets the dosimetric constraints over the whole periodic interval. Such a plan, by definition, increases the dose to the uninvolved tissues.
  - Reduction of the covered time interval compared to the total periodicity interval improves the treatment plan quality at the expense of increased treatment time.
  - For SOBP treatment fields, typically, a site-specific motion mitigation strategy can be established using, for example, ITVs or by using the most likely point in the periodicity.
  - For PBS treatment fields, the frequency of motion may interfere destructively with the spot delivery sequence and cause "interplay" effects that produce hot/cold spots in the target. Such interplay effects can only be evaluated through explicit temporal simulation of the delivery sequence in conjunction with the target motion (e.g., [53, 62, 63]).

Typical beam arrangements for various anatomical sites are summarized in Table 3.9.

3.6.2 Fraction Management

- Even a single proton field may achieve sufficient dose conformality.
- Fractions over the course of treatment may use alternating sets of one or more proton fields to decrease fraction time while maintaining, over the course, the benefit of integral dose reduction with many fields.

Table 3.9 Summary of typical beam arrangements for various anatomical sites for proton therapy plans

Site	Number of fields	Orientation	Comments
Craniospinal	4–5	Left and right posterior oblique fields to the brain, cribriform plate, and upper C-spine, with abutting PA fields to the spine	3–4 sets of these fields are planned to allow junction shifts during treatment course
Brain	2–4	Noncoplanar, multidirectional	Angles depend on tumor location and chosen to reduce integral dose and risk to OARs from end-of-range effects
Ocular melanoma	1	AP	Specialized technique with specific ocular horizontal beamline. Patient treated in seated position. Eye rotated into optimal position for OAR sparing by defining a gazing angle at simulation and indicating this on the delivery nozzle for individual patients
Head and neck, unilateral	2–3	PA/lateral/anterior oblique/ posterior oblique	Beam angles chosen to reduce integral dose or traversing heterogeneous tissue wherever possible and to reduce end-of-range effects to OAR
Head and neck, bilateral	2–3	PA/lateral/posterior oblique	Anterior beams traversing the oral cavity and nasal sinuses should be avoided wherever possible. The heterogeneity of these structures, and variation in sinus filling, increase uncertainty. Patch fields (combinations of PA and lateral fields) are often used to spare the brainstem
Breast, partial	2–3	Noncoplanar, multidirectional	Multiple beams to reduce area of skin receiving full dose and to not have all beams ranging out on the same rib

Table 3.9 (continued)

Site	Number of fields	Orientation	Comments
Breast, whole	1–2	Anterior oblique	En face, avoiding obliquity, to minimize range uncertainties caused by respiratory motion
Mediastinum/chest wall	1–2	AP/anterior oblique	En face, avoiding obliquity, to minimize range uncertainties caused by respiratory motion
Hemithorax	3	PA/posterior oblique/lateral, or AP/anterior oblique/ lateral	Beam angles depend on tumor location. Typically, three fields or used to improve plan robustness 4D CT-based treatment planning approach to account for respiratory motion
Upper GI	2–3	PA/posterior oblique	Beam angles to reduce lung/cardiac dose and to avoid traversing anatomy with significant respiratory motion
Lower GI	3	PA/posterior oblique/lateral	Avoid anatomy that varies due to bowel gas changes, stomach filling, and respiratory motion. Multiple beams increase robustness and reduce risk of end-of-range effects on radiosensitive OARs. The use of multiple angles also reduces dose to spinal cord and kidneys from entry plateau of passing beams
Prostate	2	Right and left laterals	Typically, patient treated with a full bladder and water-filled rectal balloon in situ to immobilize the prostate. Some centers utilize a spacer between the prostate and rectum instead of using a rectal balloon to spare the anterior rectal wall

- Multiple fraction groups allow for per fraction optimization of certain constraints (i.e., one fraction may allow dose to the brainstem while another must avoid it).
- The use of multiple fraction groups for a single plan requires effective support in the TPS for optimization and dose accumulation over these multiple fraction groups.

3.6.3 TPS Algorithm and Features

- A dose calculation algorithm must, at a minimum, model all the available geometric and dose-modifying features of the delivery system:
  - The user must ensure proper commissioning and use per validated protocols.
  - Extension beyond both the delivery system or calculation capabilities requires careful specification and validation.
  - Geometry features comprise those that model the position of the patient with respect to the beam axis.
  - Dosimetry features comprise those that model the beam itself, scatter effects in the patient and from external materials, apertures, range compensators, and range shifters.
- Proton dose calculation must use, at a minimum, pencil-beam algorithms (PBA):
  - The use of Monte Carlo has not yet been clinically integrated.
  - PBA, depending on their implementation, decreases in spatial resolution as a function of depth. At best, the spatial sensitivity is about 0.03ρ where ρ is the radiological depth.
  - The use of PBA in lung dose calculations should be accompanied by Monte Carlo validation (either per patient or per site standard) because of range straggling effects in the lung that are not modeled by PBA.
  - PBA should consider secondary proton interactions, where the proton interacts with the nucleus and creates a broad secondary dose effect, especially for field sizes, either confined by apertures or limited by scanning size, less than 100 mm diameter (see Fig. 3.28) [64].

The use of halo corrections often is included implicitly if patient fields are calibrated on a per field basis. The user should analyze the effect and necessity of this correction in their practice.

  - There is, theoretically, no difference in PBA for scattered, uniform scanning, or PBS fields. There may be significant implementation differences.
- Proton dose calculations (i.e., the context in which a PBA is used) must consider the effect of proton uncertainties. These include geometric and dosimetric uncertainties:
  - Geometric uncertainties are in common with those in photon radiotherapy.
  - Geometric uncertainties, however, cannot be readily accommodated by the definition of a PTV because the geometric uncertainty has an effect on the dose distribution itself unlike in photon radiotherapy.

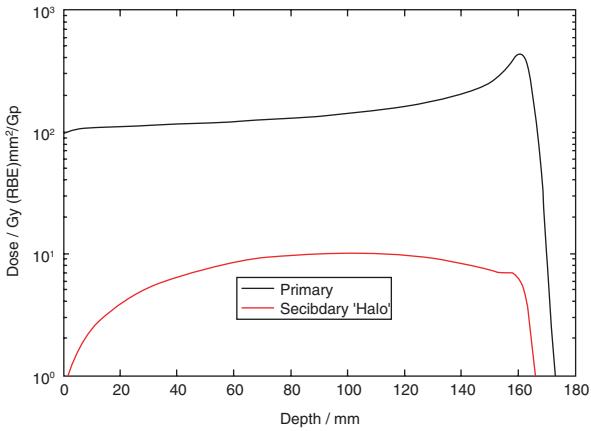

Fig. 3.28 Depth doses for primary and secondary proton dose depositions in water for an infinite broad field with infinite SAD. Note the specification of the depth dose in absolute dose per Gp. Alternatively, MU can be used as a specification in the treatment planning system. Note the use of the log scale on the ordinate axis

  - Range uncertainties (apart from those caused by geometric uncertainties) arise from uncertainty in the patient-specific (relative to water) stopping power, the proton equivalent of "attenuation." This uncertainty, in clinical practice is managed as follows:

For SOBP fields: increase of distal range penetration and decrease in proximal range penetration. Typical correction is $0.035R + 1$ mm.

- For PBS fields: the explicit modeling of variation in the isocenter position and CT values.
- Proton dose calculations currently use water-relative stopping powers (RSP) derived from CT-number-to-RSP conversion.
- The CT-number-to-RSP conversion uses a population average curve whose anchor points are (typically) water, air, and bone. This conversion carries an intrinsic uncertainty in the stopping power which contributes to the uncertainty in range.
- The dose to water calculation may differ from the effective dose to tissue [65].
- The biological equivalent proton dose relative to cobalt-60 is assumed to have an RBE = 1.1 throughout. The RBE = 1.1 is largely an empirical equivalence with minimal experimental confirmation and assumed for similar clinical end points as in photon radiotherapy. Thus, dose equivalences at extreme situations, such as in SBRT, remain subject to scrutiny.

3.6.4 PBS Optimization Volumes, Concept, and Examples

- PBS optimization computes the spot intensities, quantified in number of protons (giga-protons or Gp) or equipment-specific monitor units, such that the total dose from all spots meets the dosimetric criteria of optimization:
  - A spot is a proton pencil beam quantified by energy (range in patient), position in the isocentric plane achieved by magnetic deflection, and intensity.

  - A spot is typically "positioned" at a radiological depth equal to its distal range (typically the depth of 90% of peak value).
- An optimization algorithm typically uses a dosimetric transfer function D_{ij} that maps the dose from a unit charge to spot j to all points *i*. For that function, the dose to a point *i* is $D_i = \sum_j Q_j D_{ij}$. The use of the D_{ij} function allows the optimizer to rapidly compute the dose anywhere during the manipulation of the spot charge Q:
  - The dose calculation in PBS computes the *Dij* function prior to optimization. The patient dose is subsequently computed when the charges have been optimized.
- PBS optimization uses a spot placement algorithm that must ensure that the total set of spots of all fields can achieve the desired dosimetric result:
  - This primarily implies that the set of spots sufficiently covers the target volume, including lateral and distal extents, that ensures dose equilibrium at the target surface.
- The scale of optimization for protons is an order of magnitude larger than for photon IMRT due to the large number of spots.
- The larger solution space benefits from multi-criteria optimization (MCO) because a single-valued optimization result may, in fact, not be the most optimal in terms of clinical objectives:
  - Pareto optimization is an MCO technique that specifies a set of inviolable constraints (such as target minimum dose greater than 50 Gy(RBE)) and a set of objectives (such as, given the constraints, minimize the maximum dose to the brainstem).
  - Pareto optimization creates a multidimensional (proportional to the number of objectives) surface, the Pareto front, that contains a set of Pareto-optimal treatment plans given the constraints and treatment approach.
  - Each Pareto-optimal treatment plan is optimal given a unique set of objective values. The surface can be interrogated to assess the impact of one trade-off versus another (see Fig. 3.29).
- Current optimization techniques often require "guidance" volumes to achieve some local optimal effect. This is primarily a consequence of the limited ability to quantify the desired constraints.
- Robust optimization produces optimized plans which are insensitive, i.e., guaranteed to maintain the desired dose constraints and objectives, to uncertainties. This applies to both proton and photon optimization:
  - For photon optimization, however, robustness can be achieved through the definition of planning targets and avoidance regions around critical structures.
  - For proton optimization, the optimization must include robustness in its computation of charges.
  - Proton robust-optimized plans are currently most readily visualized through uncertainty bands around the nominal non-robust plan in a DVH (see Fig. 3.30) [66].

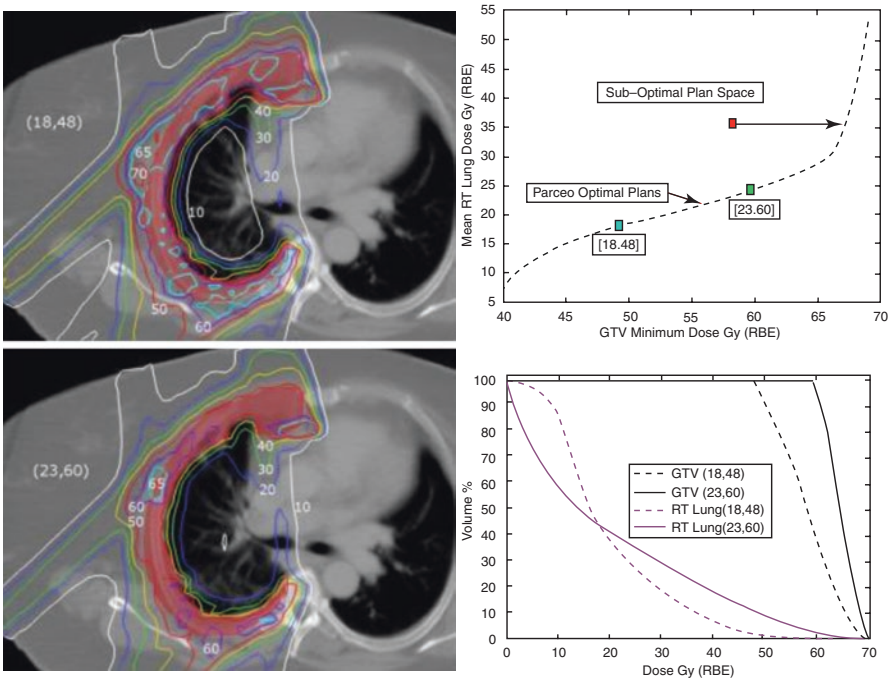

Fig. 3.29 Example trade-off analysis based on Pareto-optimal plans. Optimal mesothelioma GTV dose is in conflict with minimal lung dose. The top graph shows a curve that indicates the plans that balance the optimal trade-off of the achievable values (indicated in parentheses for two example points). The "red" point indicates a suboptimal plan because for its achieved mean lung dose, a still much higher minimum GTV dose is physically achievable. The DVHs in the bottom graph indicate the trade-off between the two plans indicated on the curve. The left figures are transverse sections for each point. The plan uses three proton PBS fields: anterior, posterior oblique, and right oblique. Patient example courtesy of Dr. Bernard Eden

3.6.5 Patient Field QA

- Patient field QA establishes that:
  - The dose in the patient is correct.
  - The dose as delivered is correct.
- The dose in patient can only be validated by an independent dose calculation method. Monte Carlo is assumed to be most accurate and even in excess compared to the dose calculation. The use of Monte Carlo, however, requires careful validation of the Monte Carlo itself.
- The delivered dose validation is established by tracing the field and dose information from its origin in the TPS, its transfer to the delivery system, and its measurement by an independent, traceable to standards, measuring device:
  - The measurements require an equivalent dose representation in the TPS and on the delivery system. This is achieved most easily in a water-equivalent phantom.

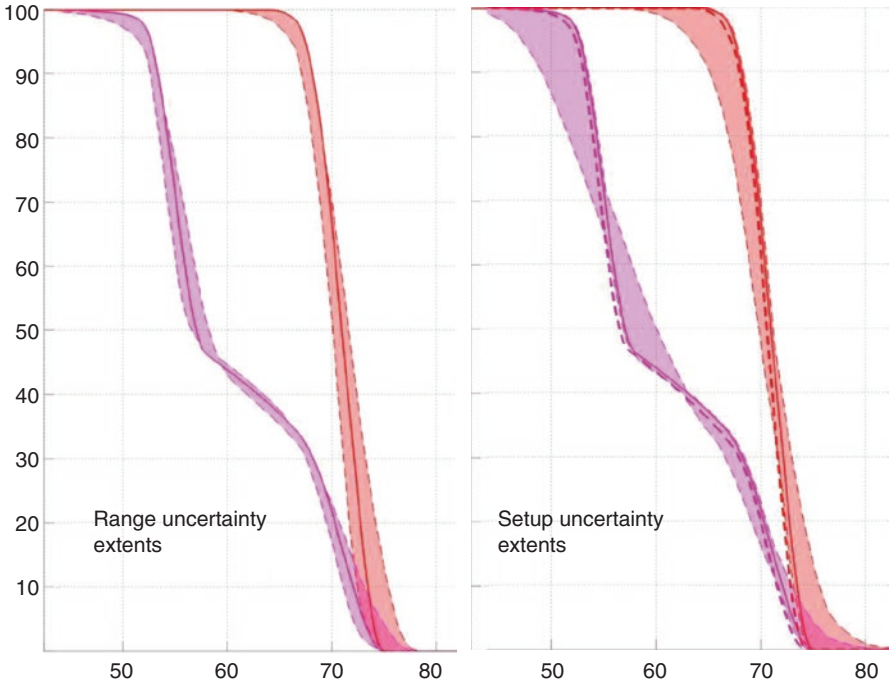

Fig. 3.30 DVHs for nominal case (*solid line*) and maximum extents given range uncertainty (*left*) and setup uncertainty (*right*). Note that the setup uncertainty has a larger effect. The setup uncertainty, if random over multiple treatment fractions N, will be reduced by approximately $\sqrt{N}$ and thus become much smaller

- Note that such a measurement may not validate consequences of inpatient heterogeneities which can only be validated through Monte Carlo.
- The measurement should quantify the three-dimensional features of the dose distribution which typically requires the measurement in at least two planes.
- The measurement should include field specific devices such as range shifter or aperture.
- Dose equivalence is established by a spatially/dosimetrically sensitive algorithm. Most commonly, the γ-index is applied. Of particular relevance is the 3D γ-index [67].

3.7 SRS Treatment Planning

- Stereotactic radiosurgery is a proven treatment modality in photon clinics with both cobalt (Gamma Knife) and traditional, gimbaled, and robotic linear accelerator systems. As opposed to traditional fractionation schedules that are gener-

ally accepted to increase the therapeutic ratio based upon the four Rs of radiobiology, photon SRS treatments rely upon a single fraction of high dose delivered to a highly localized region that achieves a therapeutic ratio by the geometric avoidance of healthy tissue. With proton SRS, the therapeutic ratio is identically determined by the localization of a high dose delivered to a targeted region and the dosimetric sparing of healthy tissues.

- In the case of proton-based SRS treatments, the dose delivered to the target is prescribed to the same level as photon therapies. The normalization level is institution specific and controls the amount of dose heterogeneity inside the targeted region.
- Proton SRS can generally achieve greater dose homogeneity due to the specifics of the dose delivery techniques compared (scattered or scanned beams) to linear accelerator-based treatments (cones and small MLC shapes).
- For smaller treatment targets, the proton-beam profiles are dominated by penumbra due to the lateral scattering of the protons as they pass through tissue. Similar to photons, the size of the penumbra increases with depth in tissue. Unlike photons, the penumbra of the proton fields is dependent more on depth and field size. For proton SRS, the penumbra is affected by field size, depth, range, apertures, range compensators, air gap, effective source position (beam optics), and tissue heterogeneities (Fig. 3.31).

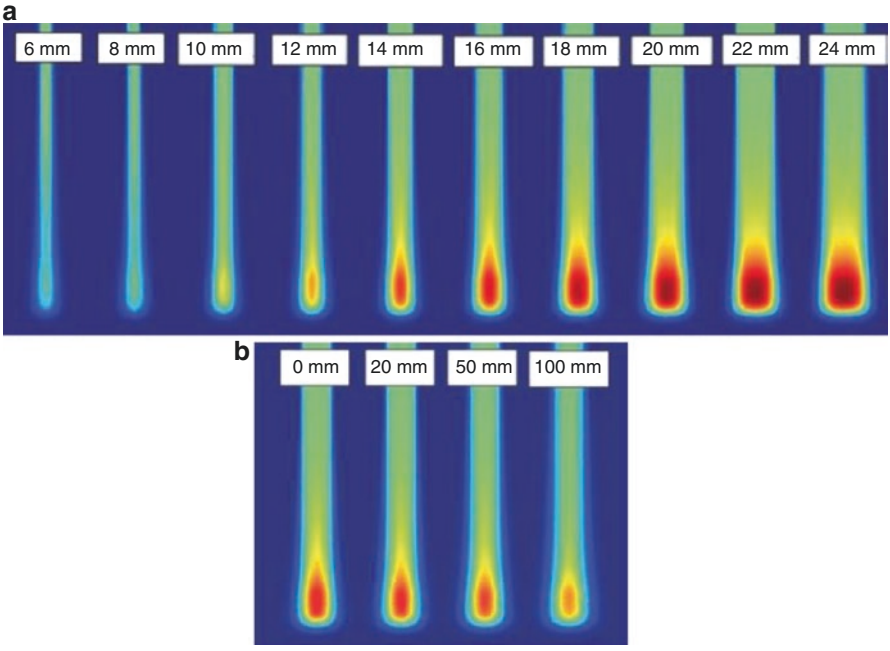

Fig. 3.31 Two factors that affect the penumbra: field size (**a**) and air gap (**b**)

3.7.1 Treatment Planning Considerations for Proton SRS

The above issues must be addressed in the commissioning of a proton SRS program and properly modeled in the treatment planning system or corrected prior to beam delivery. Additionally, treatment planning protocols can reduce the effects of scattering and penumbra through the use of beam angle optimization, limits on the minimum field sizes or target sizes, and the use of multiple treatment beams (Table 3.10). Such planning protocols will increase dose conformality to the GTV, reduce delivery uncertainty effects, and increase treatment robustness.

3.7.2 Proton SRS with Scattered Beam

- Current state-of-the-art proton SRS utilizes scattering delivery systems since scanning systems are only recently becoming more available. Treatment planning protocols employ apertures and range compensators to increase conformality in the lateral and distal directions.
- Planning for cranial SRS always includes at least two treatment beams and frequently three or more to increase conformality and plan robustness.
- The air gap is minimized to sharpen the penumbra, both geometric penumbra and scattering penumbra; and beam angles are selected to minimize tissue heterogeneities and distal edge sparing of critical organs.

3.7.3 Proton SRS with Scanned Beam

- While scanning is not widely utilized in proton SRS programs, it is expected to increase as more scanning rooms enter clinical use and proton SRS programs are commissioned in new treatment rooms.
- Scanned beam proton SRS will increase the proximal conformality of proton SRS treatments.
- There may be clinical scenarios wherein physical apertures may sharpen the penumbra and increase conformality for scanned beam proton SRS delivery and

Table 3.10 A summary of common uncertainties that can be minimized with planning protocols

Effect	Treatment planning mitigation technique
Scattering and penumbra reduce target dose	Minimum field size for treatments
Range variation increases dose to organs	Avoid distal sparing of organs
Scattering from tissue heterogeneities	Avoid beam angles parallel to tissue boundaries
Lack of dose conformality	Increase number of beams
Large dose uncertainty from a single beam angle	Increase number of beams
Range uncertainties	Beam-specific margins and/or robust optimization

should be considered in the treatment planning process if apertures are available at the institution. Range compensators may also increase the distal conformality of the scanned delivery.

- Since many SRS treatment targets are small, SFUD planning techniques are often the first option for treatment planning unless there is desire to incorporate a simultaneous integrated boost (SIB) for a GTV/CTV.
- Proton SRS can provide the clinical tools to treat more complicated target geometries that are not possible with traditional photon SRS tools. Examples which lend themselves to proton SRS as opposed to photon are indicated in Sect. 7.5. In these cases, IMPT may be considered but may introduce additional delivery uncertainties and reduced plan robustness that cannot be compensated with fractionation.

3.7.4 Commissioning and QA Considerations Specific for Proton SRS

- Commissioning of a proton SRS program must include percent depth dose (PDD) and profile measurements of small proton fields and single pencil beams.
- Some treatment planning systems only allow for an integrated depth dose (IDD) measurement which does not capture the penumbral variations, instead relying upon a deconvolution model to determine the penumbra (Fig. 3.32). While the deconvolution method can model small proton fields and single pencil beams, the model must be validated against measurements.
- The measurements must use appropriate detectors that minimize volume averaging and LET affects.
- Additional considerations for commissioning should include uncertainty analysis of all isocenters (beam, mechanical, imaging, patient positioner, etc.), specifically the coincidence of all isocenters to the radiation isocenter.
- A final component for commissioning an SRS program must include a robust end-to-end test utilizing one of the many SRS phantoms currently available. The phantom should allow for the testing of various treatment depths and target sizes

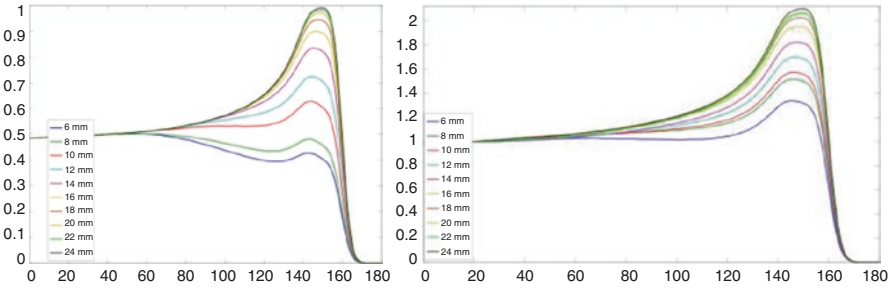

Fig. 3.32 A comparison of a PDD (*left*) and an IDD (*right*) for an SOBP with identical range and modulation but for different field sizes

and not introduce additional treatment delivery uncertainties such as SPR uncertainties from unknown plastics or oversimplified geometries that fail to test the image guidance systems.

3.7.5 Clinical Benefits of Physical Dose Properties of Proton SRS

- Given a commissioned proton SRS treatment program, the clinical benefits of proton SRS can be considered from two patient cohorts: benign and metastatic. The physical dose delivery advantage of protons versus photons is well documented in the integral dose delivered to healthy tissues.
- For superficial targets in the cranial cavity such as meningiomas near the outer surface of the cranial cavity, the integral dose to healthy tissues is zero after the distal falloff which is generally within millimeters from the distal edge of the target.
- For more centrally located targets, the integral dose difference between protons and photons is most pronounced below the 40% isodose level, assuming identical prescription doses.
- The high-dose regions, above the 40% isodose levels, are generally very similar, except that the higher dimensional planning variables of proton therapy optimization can allow for better shaping of high-dose regions when a target is in close proximity to a critical structure, especially in the case of complicated target geometries in close proximity to critical structures.

3.7.6 Benign Lesions

For benign lesions, the effects of the integral dose should be considered in the clinical evaluation of the patient's treatment options and may affect the risk of late effects of the radiation treatment. Additionally, the ability of proton therapy to increase the conformality of high-dose regions in complicated target geometries, especially when the target is in close proximity to a critical structure, should be considered in the evaluation of treatment options (Fig. 3.33).

3.7.7 Metastatic Lesions

- The benefits of reduced integral dose are not well documented for patients with metastatic lesions, and the differences of proton SRS versus photon SRS for metastatic patients can be physically described in two scenarios, regardless of the clinical benefit or need.
- There are some cases where proton SRS can reduce the high dose to critical organs for cases when the target is in close proximity to the critical organ or has a complex geometric relationship with the critical organ. The other physical difference is the reduction of brain integral dose for multiple metastatic lesions (Fig. 3.34). The clinical necessity for these physical differences is outside the scope of this section.

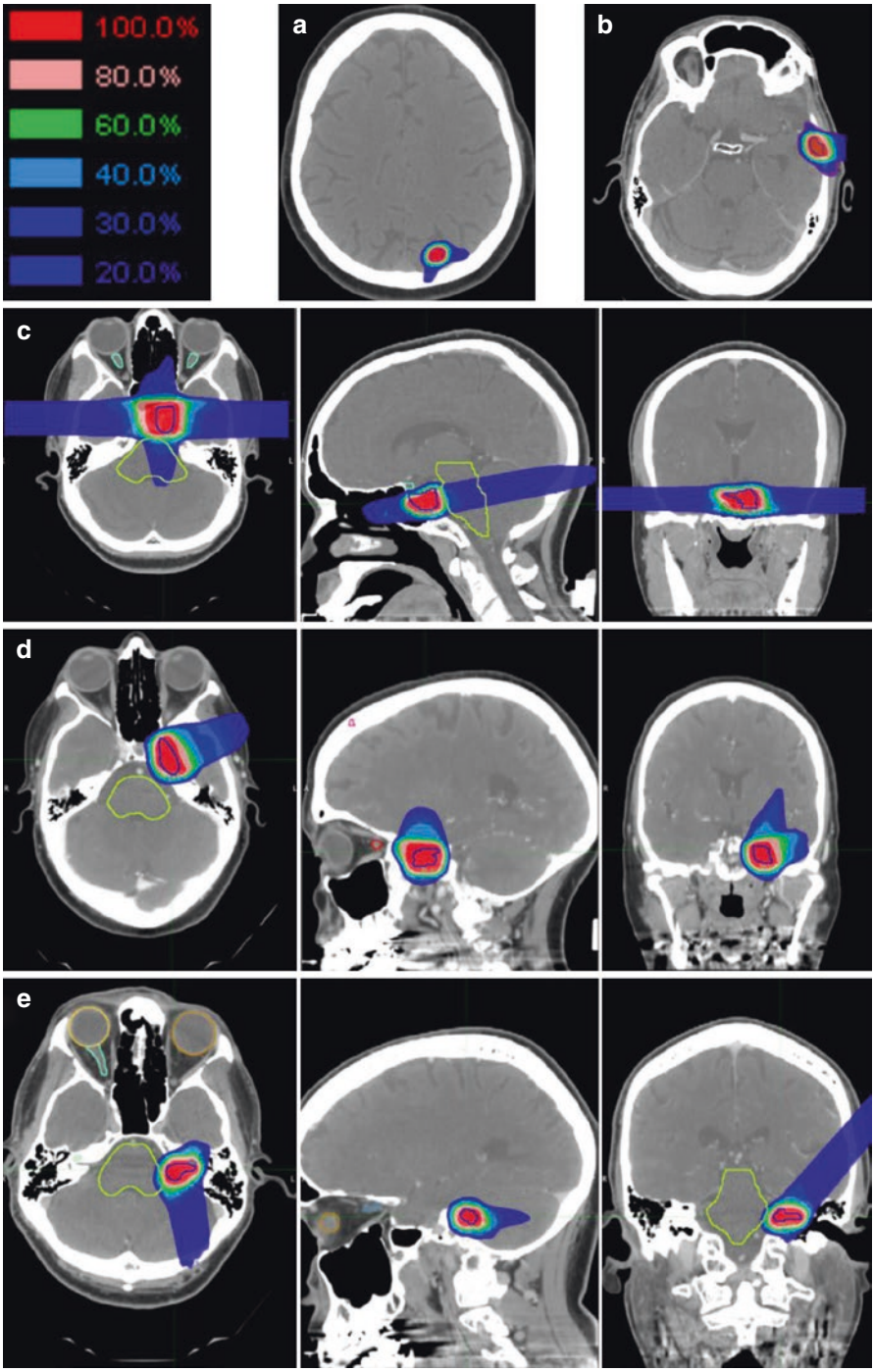

Fig. 3.33 Examples of benign lesions treated with proton SRS. The relative dose legend is displayed in the top row for all images. Displayed are axial images of an AVM (**a**) and a meningioma (**b**). Axial, sagittal, and coronal images are supplied for a pituitary target (**c**), a more central meningioma (**d**), and a cerebellopontine angle lesion (**e**)

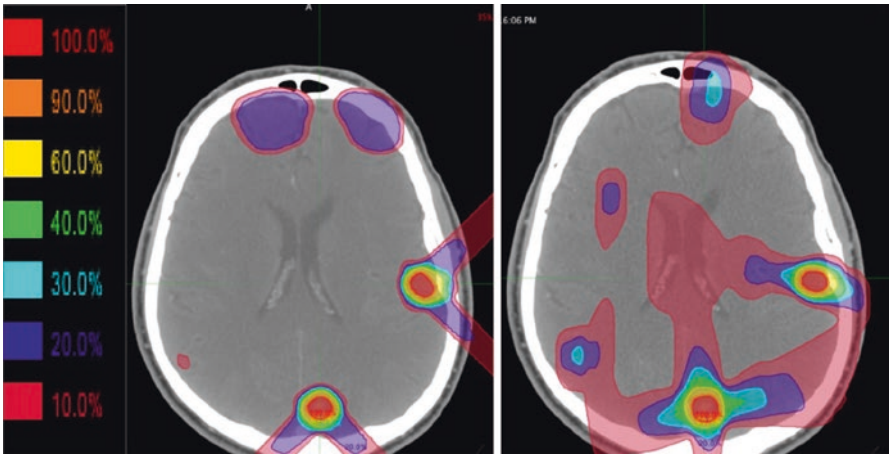

Fig. 3.34 A comparison of a proton SRS (*left*) and a photon SRS (*right*) plan for a patient with multiple metastatic lesions. The difference of integral dose to the brain can be observed

3.8 Image Guided Radiation Therapy (IGRT)

3.8.1 Purpose

IGRT generally refers to frequent, serial imaging of some kind performed in the treatment room prior to delivery of RT. The main purpose of IGRT is better localization of target and normal tissue volumes and thereby reducing uncertainty (PTV margins) and avoiding missing the tumor or overexposing OARs. For protons, it is also essential to verify the path length of proton beams.

IGRT strategies can be broadly divided into online and offline approaches. Online patient position verification and correction is *standard* in particle therapy. Setup correction protocols are routinely used. The most recent information is used in the process in order to ensure accurate delivery of treatment.

In the past 15 years, IGRT for X-ray therapy has evolved and matured with the advances in electronic portal imaging devices, kV radiographic systems, CBCT, and MR linacs. In contrast, proton therapy IGRT has lagged behind.

A summary of imaging techniques for proton therapy has been presented in Chap. 2. The relevance of various modalities to IGRT is discussed in this section.

3.8.2 In-Room Digital Radiography

- In-room digital radiography and orthogonal pair of X-ray tubes and digital flat panel imagers are the minimum requirements for proton therapy.
- 2D-2D alignment based on DRRs and comparison of anatomical landmarks (e.g., bony anatomy) is still the most commonly used IGRT technique in proton therapy.

- Alignment algorithms can be automatic or interactive.
- The system may support the real-time monitoring and verification of the patient during fluoroscopy and respiratory gated treatment.

3.8.3 Out-of-Room CT

- Out-of-room CT is based on the use of a remote positioning and imaging system.
- Saves valuable room time for irradiation of patients.
- Some patient motion may be induced because of the transportation system.

3.8.4 Radiopaque Markers [68]

- Allows for patient setup with respect to the tumor itself instead of bony anatomy.
- Gold helical markers (10 mm length; 0.35 mm, 0.75 mm, 1.15 mm diameters).
- Dose perturbations of 31% (1.15 mm diameter) versus 23% (0.75 mm diameter) for typical lateral-opposed beams.
- Dose perturbation is not observed for 0.35 mm markers; however, they are deemed too fragile for implantation.
- Magnitude of dose perturbation depends on marker size, orientation, and distance from the beam's end of range.

3.8.5 In-Room CT [69]

- Necessary for target positioning and range verification.
- Used in vertical position for seated patients.
- Used in conjunction with a treatment couch robot on a six-axis robot.
- In-room robotic couch can transport the patient between the beam gantry and CT scanner.
- Portable large bore CT scanners are available as well.

3.8.6 CBCT

- It is expected that 2D radiography will continue to be used for proton IGRT in the foreseeable future.
- CBCT is now starting to be employed at some centers and is expected to be installed in most new installations in the next few years mostly for more precise patient positioning and adaptive radiotherapy [70].
- CBCT has the added advantage of visualizing soft tissue changes, which is important for adaptive proton RT, especially for head and neck tumors
- CBCT is, however, not accurate enough for proton plan assessment before treatment.

3.8.7 CT on Rails

- CT on rails can provide diagnostic quality imaging and has recently been installed in several proton centers.
- A robot moves the patient to imaging isocenter.
- The CT scanner translates over patient for imaging.
- A robot moves patient back to treatment position, while CT reconstruction/registration is performed.
- CT on rails will have use in adaptive replanning, particularly for head and neck cases.

3.8.8 Other Auxiliary Methods

3.8.8.1 Ultrasound

- In-room ultrasound pretreatment alignment is used for some prostate, lung, abdominal, and breast tumor sites. The most experience exists with interfractional tracking for prostate cancer
- AAPM TG 154: QA of US-guided EBRT for prostate cancer

3.8.8.2 Optical Systems

- Optical systems allow surface tracking with ceiling-mounted camera systems in the simulation and treatment rooms.
- These systems can detect intrafractional motion.
- They use rigid body transformations in combination with a least-square fit to minimize the difference between the actual expected surface.
- There are currently two commercial systems available (AlignRT and C-RAD sentinel).
- AAPM TG 147: QA of nonradiographic RT localization and positioning systems.

3.8.8.3 Radio-frequency Systems

- Only one commercial system (Calypso) available
- Currently not used in proton therapy due to potential interference of transponder beacons with proton dose distribution

3.8.8.4 Prompt Gamma Imaging

- Elemental prompt gamma (PG) rays arise during proton irradiation of tissue.
- PG ray lines are specific for the excited nucleus.
- The intensity and profile of the PG ray emission are strongly correlated to delivered dose and Bragg peak position.
- Compton cameras for PG detection and intratreatment beam range verification are under development.

3.8.8.5 Proton Radiography and CT [16]

- Proton radiography and proton CT traverse the patient with a proton beam and measure residual energy at exit.
- Proton radiography and proton CT are emerging technologies with promising properties.
- Proton radiography could track lung tumors in real time providing accurate validations of tumor motion models.
- Proton CT would provide a direct map of stopping power.
- Proton CT would provide accurate 3D maps of the patient just before treatment, opening the possibility of low-dose daily imaging for adaptive proton RT.
- First clinical systems are under development and should become available in the coming years.

3.8.8.6 PET

- PET of proton-activated isotopes has been shown to be valuable for range verification during and after treatment.
- In soft tissues, the most important radionuclide species are 11 C (half-life 20 min), 13 N (half-life 10 min), and 15 O (half-life 122 s), of which 15 O is dominant but decays fastest.
- The PET-detected activation can be compared with the expected radioactivity distribution.
- This method may serve as an in vivo, noninvasive range validation method of the entire chain of treatment planning and delivery.
- Three operational modalities are currently in use:
  - In-beam PET with modified detectors to synchronize acquisition with beam delivery during treatment
  - In-room portable PET, posttreatment
  - Offline detection of residual activation from long-lived emitters shortly after treatment, taking into consideration the physical and biological decay

3.8.8.7 Repeated 4D CT Scanning

- Treatment planning CT is just a snapshot in time before the actual treatment course.
- The patient may breathe differently or have varying breathing amplitudes over the treatment course.
- Tumor growth or shrinkage, atelectasis, radiation pneumonitis, and pericardial effusion may further change the anatomy, resulting in an altered dose distribution.
- Repeated 4D CT scanning minimizes the probability of severe geometric misses.
- 4D CTs are typically done every other week.

3.8.9 Impact of Anatomical Changes and Adaptive Radiotherapy

- Proton plans are sensitive to intrafractional variations, even with proper image-guided setup:
  - Tumor growth can cause underdosing of tumor.
  - Tumor shrinkage can cause protons to overshoot into an OAR.
  - Weight gain can cause under dosing of a distal target.
- Proton plans are more sensitive than photon plans since dose distribution can change significantly, intrinsically due to the 3D modulation of proton beam, as opposed to 2D modulation of photon beam.
- ART (adaptive radiotherapy) can correct the dosimetric effect of nonrigid anatomical changes, complementing the ability of image-guided setup to correct for rigid body translation and rotation.
- Frequency of treatment adaptation is limited by technological availability of (in-room) volumetric imaging as well as time and resources.

3.9 Emerging Technologies and Future Developments

There are two aims that drive innovation and new technologies in proton radiotherapy:

1. Leveraging the unique properties of proton (and ion) radiation
2. Decreasing the effective cost of proton radiotherapy:
   The unique properties of proton (and ion) radiation allow for:
   (a) New in vivo imaging techniques by using the proton pencil beam itself as a measurement probe. Examples include:
      - Prompt γ detection to determine the range penetration in patient and perhaps a certain level of elemental tissue composition because different atoms release different γ energies.
      - Proton radiography to image stopping power changes in the patient and to improve stopping power determination in the patient:
        - Proton tomography, by itself, may not emerge as an effective imaging means due to inpatient scattering of the proton beam. Techniques that use a combination of high-resolution CT and a limited set of proton radiographs may, in fact, be better.
        - Continued advances in CT such as multispectral analysis may be more practical and even more accurate.

   (b) Biological treatment modulation. We currently assume a constant RBE = 1.1 throughout the dose distribution. For protons, the LET effect occurs at the distal falling edge of the dose distribution. Its effect, however, is believed to be of significance. Analysis of the LET distribution may yield some clinical considerations.

It must be noted that the proton delivery system is a fully electronic system where the scanning magnet moves the beam in the lateral dimension and proton energy changes the depth of penetration. Thus, compared to a mechanical MLC system, the delivery system is:

1. Faster
2. More reliable
3. Easier to control in real time to adapt the pattern to match the patient state during treatment

In addition, the proton spot map specifies each spot in terms of energy, location, and intensity. The control system directly (i.e., commutatively) uses these parameters to control the delivery and directly measures the same parameters. Thus, the feedback loop between delivery, measure, and adapt does not suffer from intermediate conversion. In contrast, an MLC uses leaf positions to specify MU which is certainly neither an obvious nor unique (i.e., commutative) translation. This is a clear technological advantage for proton radiotherapy in consideration of dynamic delivery requirements.

The effective cost of proton radiotherapy may be reduced when considering desired advances in radiotherapy in general. These include:

1. IGRT—Image-guided radiotherapy and synchronized dynamic beam delivery:
   (a) The ability to use the proton beam, itself, as a direct measure of where the beam is in the patient's anatomy, creates new opportunities to control the motion.
2. ART to correct for changes in the patient:
   (a) ART primarily requires novel software architectures to allow for continuous data communication in response to patient changes. These architectures must implement DICOM second generation to address the temporal synchronization of the flow of data.
   (b) Proton ART will benefit from the superior delivery technology which will allow the adaptation to occur within the treatment session.
3. SBRT—Increase in fraction dose with concomitant reduction in treatment course length:
   (a) Clearly, the reduction in the dose bath (by approximately 1/2) will favor dose escalation with protons. Thus, proton SBRT should effectively compete and should allow a cost reduction in patient treatment length.

References

1. Bortfeld T. An analytical approximation of the Bragg curve for therapeutic proton beams. Med Phys. 1997;24(12):2024–33.
2. ICRU. ICRU Report 78: prescribing, recording, and reporting proton-beam therapy. J ICRU. 2007;7(2):1–210.
3. Khan FM, Gerbi BJ. Treatment planning in radiation oncology. Philadelphia: Wolters Kluwer Health/Lippincott Williams & Wilkins; 2012.
4. Moyers MF, Miller DW, Bush DA, Slater JD. Methodologies and tools for proton beam design for lung tumors. Int J Radiat Oncol Biol Phys. 2001;49(5):1429–38.

5. Moyers MF, Sardesai M, Sun S, Miller DW. Ion stopping powers and CT numbers. Med Dosim. 2010;35(3):179–94.
6. Yang M, Zhu XR, Park PC, Titt U, Mohan R, Virshup G, Clayton JE, Dong L. Comprehensive analysis of proton range uncertainties related to patient stopping-power-ratio estimation using the stoichiometric calibration. Phys Med Biol. 2012;57(13):4095.
7. Wu R, Amos R, Sahoo N, Kornguth D, Bluett J, Gillin M, Zhu X. SU-GG-J-80: effect of CT truncation artifacts to proton dose calculation. Med Phys. 2008;35(6):2697.
8. Moyers MF, Miller DW. Range, range modulation, and field radius requirements for proton therapy of prostate cancer. Technol Cancer Res Treat. 2003;2(5):445–7.
9. Yu Z, Bluett J, Zhang Y, Zhu X, Lii M, Mohan R, Dong L. SU-GG-T-470: impact of daily patient setup variation on proton beams passing through the couch edge. Med Phys. 2010;37(6):3294.
10. Paganetti H, Niemierko A, Ancukiewicz M, Gerweck LE, Goitein M, Loeffler JS, Suit HD. Relative biological effectiveness (RBE) values for proton beam therapy. Int J Radiat Oncol Biol Phys. 2002;53(2):407–21.
11. Paganetti H. Relative biological effectiveness (RBE) values for proton beam therapy. Variations as a function of biological endpoint, dose, and linear energy transfer. Phys Med Biol. 2014;59(22):R419.
12. Woodward WA, Amos RA. Proton radiation biology considerations for radiation oncologists. Int J Radiat Oncol Biol Phys. 2016;95(1):59–61.
13. Schneider U, Pedroni E, Lomax A. The calibration of CT Hounsfield units for radiotherapy treatment planning. Phys Med Biol. 1996;41(1):111.
14. Schaffner B, Pedroni E. The precision of proton range calculations in proton radiotherapy treatment planning: experimental verification of the relation between CT-HU and proton stopping power. Phys Med Biol. 1998;43(6):1579.
15. van Elmpt W, Landry G, Das M, Verhaegen F. Dual energy CT in radiotherapy: current applications and future outlook. Radiother Oncol. 2016;119(1):137–44.
16. Testa M, Verburg JM, Rose M, Min CH, Tang S, Bentefour EH, Paganetti H, Lu H-M. Proton radiography and proton computed tomography based on time-resolved dose measurements. Phys Med Biol. 2013;58(22):8215.
17. ICRP. ICRP Publication 23: Report of the Task Group on Reference Man. 1975.
18. ICRU. ICRU Report 44: Tissue substitutes in radiation dosimetry and measurement. 1989.
19. Schneider W, Bortfeld T, Schlegel W. Correlation between CT numbers and tissue parameters needed for Monte Carlo simulations of clinical dose distributions. Phys Med Biol. 2000;45(2):459.
20. Hansen DC, Seco J, Sørensen TS, Petersen JBB, Wildberger JE, Verhaegen F, Landry G. A simulation study on proton computed tomography (CT) stopping power accuracy using dual energy CT scans as benchmark. Acta Oncol. 2015;54(9):1638–42.
21. Hünemohr N, Paganetti H, Greilich S, Jäkel O, Seco J. Tissue decomposition from dual energy CT data for MC based dose calculation in particle therapy. Med Phys. 2014;41(6):061714.
22. Taasti VT, Høye EM, Hansen DC, Muren LP, Thygesen J, Skyt PS, Balling P, Bassler N, Grau C, Mierzwińska G, Rydygier M, Swakoń J, Olko P, Petersen JBB. Technical note: improving proton stopping power ratio determination for a deformable silicone-based 3D dosimeter using dual energy CT. Med Phys. 2016;43(6):2780–4.
23. Zhu J, Penfold SN. Dosimetric comparison of stopping power calibration with dual-energy CT and single-energy CT in proton therapy treatment planning. Med Phys. 2016;43(6):2845–54.
24. Wertz H, Jäkel O. Influence of iodine contrast agent on the range of ion beams for radiotherapy. Med Phys. 2004;31(4):767–73.
25. Hanley J, Debois MM, Mah D, Mageras GS, Raben A, Rosenzweig K, Mychalczak B, Schwartz LH, Gloeggler PJ, Lutz W, Ling CC, Leibel SA, Fuks Z, Kutcher GJ. Deep inspiration breath-hold technique for lung tumors: the potential value of target immobilization and reduced lung density in dose escalation. Int J Radiat Oncol Biol Phys. 1999;45(3):603–11.
26. Mah D, Hanley J, Rosenzweig KE, Yorke E, Braban L, Ling CC, Leibel SA, Mageras G. Technical aspects of the deep inspirational breath-hold technique in the treatment of thoracic cancer. Int J Radiat Oncol Biol Phys. 2000;48(4):1175–85.

27. Paoli J, Rosenzweig KE, Yorke E, Hanley J, Mah D, Ma jeras GS, Hunt MA, Braban LE, Liebel SA, Ling CC. Comparison of different respiratory levels in the treatment of lung cancer: implications for gated treatment. Int J Radiat Oncol Biol Phys. 1999;45(3):386–7.
28. Mageras GS, Yorke E. Deep inspiration breath hold and respiratory gating strategies for reducing organ motion in radiation treatment. Semin Radiat Oncol. 2004;14:65–75. Elsevier.
29. DeLaney TF, Kooy HM, editors. Proton and charged particle radiotherapy. Philadelphia: Lippincott Williams & Wilkins; 2008.
30. Olch AJ, Gerig L, Li H, Mihaylov I, Morgan A. Dosimetric effects caused by couch tops and immobilization devices: report of AAPM task group 176. Med Phys. 2014;41(6):061501.
31. Wang P, Yin L, Zhang Y, Kirk M, Song G, Ahn PH, Lin A, Gee J, Dolney D, Solberg TD, Maughan R, McDonough J, Teo B-KK. Quantitative assessment of anatomical change using a virtual proton depth radiograph for adaptive head and neck proton therapy. J Appl Clin Med Phys. 2016;17(2):5819.
32. Both S, Shen J, Kirk M, Lin L, Tang S, Alonso-Basanta M, Lustig R, Lin H, Deville C, Hill-Kayser C, Tochner Z, McDonough J. Development and clinical implementation of a universal bolus to maintain spot size during delivery of base of skull pencil beam scanning proton therapy. Int J Radiat Oncol Biol Phys. 2014;90(1):79–84.
33. Shen J, Liu W, Anand A, Stoker JB, Ding X, Fatyga M, Herman MG, Bues M. Impact of range shifter material on proton pencil beam spot characteristics. Med Phys. 2015;42(3): 1335–40.
34. Both S, Wang KK, Plastaras JP, Deville C, Ad VB, Tochner Z, Vapiwala N. Real-time study of prostate intrafraction motion during external beam radiotherapy with daily endorectal balloon. Int J Radiat Oncol Biol Phys. 2011;81(5):1302–9.
35. Wang KK, Vapiwala N, Deville C, Plastaras JP, Scheuermann R, Lin H, Bar. Ad V, Tochner Z, Both S. A study to quantify the effectiveness of daily endorectal balloon for prostate intrafraction motion management. Int J Radiat Oncol Biol Phys. 2012;83(3):1055–63.
36. Taku N, Yin L, Teo B, Lin LL. Quantifying vaginal motion associated with daily endorectal balloon during whole pelvis radiation therapy for gynecologic cancers. Int J Radiat Oncol Biol Phys. 2014;90(1):S506.
37. Zou W, Lin H, Plastaras JP, Wang H, Bui V, Vapiwala N, McDonough J, Touchner Z, Both S. A clinically feasible method for the detection of potential collision in proton therapy. Med Phys. 2012;39(11):7094–101.
38. Brock K. TU-E-BRB-03: overview of proposed TG-132 recommendations. Med Phys. 2015;42(6):–3618.
39. Graves YJ, Smith A-A, Mcilvena D, Manilay Z, Lai YK, Rice R, Mell L, Jia X, Jiang SB, Cervinõ L. A deformable head and neck phantom with in-vivo dosimetry for adaptive radiotherapy quality assurance. Med Phys. 2015;42(4):1490–7.
40. Dice LR. Measures of the amount of ecologic association between species. Ecology. 1945;26(3):297–302.
41. Huttenlocher DP, Klanderman GA, Rucklidge WJ. Comparing images using the Hausdorff distance. IEEE T Pattern Anal. 1993;15(9):850–63.
42. Christensen GE, Johnson HJ. Invertibility and transitivity analysis for nonrigid image registration. J Electron Imaging. 2003;12(1):106–17.
43. Saleh ZH, Apte AP, Sharp GC, Shusharina NP, Wang Y, Veeraraghavan H, Thor M, Muren LP, Rao SS, Lee NY, Deasy JO. The distance discordance metric—a novel approach to quantifying spatial uncertainties in intra-and inter-patient deformable image registration. Phys Med Biol. 2014;59(3):733.
44. Schreibmann E, Pantalone P, Waller A, Fox T. A measure to evaluate deformable registration fields in clinical settings. J Appl Clin Med Phys. 2012;13(5):3829.
45. Varadhan R, Karangelis G, Krishnan K, Hui S. A framework for deformable image registration validation in radiotherapy clinical applications. J Appl Clin Med Phys. 2013;14(1): 4066.
46. Brock KK. Results of a multi-institution deformable registration accuracy study (MIDRAS). Int J Radiat Oncol Biol Phys. 2010;76(2):583–96.

47. Nielsen MS, Østergaard LR, Carl J. A new method to validate thoracic CT-CT deformable image registration using auto-segmented 3D anatomical landmarks. Acta Oncol. 2015;54(9):1515–20.
48. B. Rigaud, A. Simon, J. Castelli, M. Gobeli, J.-D. Ospina Arango, G. Cazoulat, O. Henry, P. Haigron, and R. De Crevoisier. Evaluation of deformable image registration methods for dose monitoring in head and neck radiotherapy. Biomed Res Int, 2015;2015.
49. Yazdia M, Gingras L, Beaulieu L. An adaptive approach to metal artifact reduction in helical computed tomography for radiation therapy treatment planning: experimental and clinical studies. Int J Radiat Oncol Biol Phys. 2005;62(4):1224–31.
50. Axente M, Paidi A, Von Eyben R, Zeng C, Bani-Hashemi A, Krauss A, Hristov D. Clinical evaluation of the iterative metal artifact reduction algorithm for CT simulation in radiotherapy. Med Phys. 2015;42(3):1170–83.
51. Dietlicher I, Casiraghi M, Ares C, Bolsi A, Weber DC, Lomax AJ, Albertini F. The effect of surgical titanium rods on proton therapy delivered for cervical bone tumors: experimental validation using an anthropomorphic phantom. Phys Med Biol. 2014;59(23):7181.
52. Kang Y, Zhang X, Chang JY, Wang H, Wei X, Liao Z, Komaki R, Cox JD, Balter PA, Liu H, Zhu XR, Mohan R, Dong L. 4D proton treatment planning strategy for mobile lung tumors. Int J Radiat Oncol Biol Phys. 2007;67(3):906–14.
53. Dowdell S, Grassberger C, Sharp GC, Paganetti H. Interplay effects in proton scanning for lung: a 4D Monte Carlo study assessing the impact of tumor and beam delivery parameters. Phys Med Biol. 2013;58:4137–56.
54. Park PC, Zhu XR, Lee AK, Sahoo N, Melancon AD, Zhang L, Dong L. A beam-specific planning target volume (PTV) design for proton therapy to account for setup and range uncertainties. Int J Radiat Oncol Biol Phys. 2012;82(2):e329–36.
55. Goitein M. Compensation for inhomogeneities in charged particle radiotherapy using computed tomography. Int J Radiat Oncol Biol Phys. 1978;4(5):499–508.
56. Urie M, Goitein M, Wagner M. Compensating for heterogeneities in proton radiation therapy. Phys Med Biol. 1984;29(5):553.
57. Strom EA, Amos RA, Shaitelman SF, Kerr MD, Hoffman KE, Smith BD, Tereffe W, Stauder MC, Perkins GH, Amin MD, Wang X, Poenisch F, Ovalle V, Buchholz TA, Babiera G, Woodward WA. Proton partial breast irradiation in the supine position: treatment description and reproducibility of a multibeam technique. Pract Radiat Oncol. 2015;5(4):e283–90.
58. Giebeler A, Newhauser WD, Amos RA, Mahajan A, Homann K, Howell RM. Standardized treatment planning methodology for passively scattered proton craniospinal irradiation. Radiat Oncol. 2013;8(1):1.
59. Stoker J, Amos R, Li Y, Liu W, Park P, Sahoo N, Zhang X, Zhu X, Gillin M. SU-E-T-693: comparison of discrete spot scanning and passive scattering craniospinal proton irradiation. Med Phys. 2013;40(6):365.
60. Lin H, Ding X, Kirk M, Liu H, Zhai H, Hill-Kayser CE, Lustig RA, Tochner Z, Both S, McDonough J. Supine craniospinal irradiation using a proton pencil beam scanning technique without match line changes for field junctions. Int J Radiat Oncol Biol Phys. 2014;90(1):71–8.
61. Li Y, Zhang X, Dong L, Mohan R. A novel patch-field design using an optimized grid filter for passively scattered proton beams. Phys Med Biol. 2007;52(12):N265.
62. Li Y, Kardar L, Li X, Li H, Cao W, Chang JY, Liao L, Zhu RX, Sahoo N, Gillin M, Liao Z, Komaki R, Cox JD, Lim G, Zhang X. On the interplay effects with proton scanning beams in stage III lung cancer. Med Phys. 2014;41(2):021721.
63. Zeng C, Plastaras JP, Tochner ZA, White BM, Hill-Kayser CE, Hahn SM, Both S. Proton pencil beam scanning for mediastinal lymphoma: the impact of interplay between target motion and beam scanning. Phys Med Biol. 2015;60:3013–29.
64. Clasie B, Depauw N, Fransen M, Gomà C, Panahandeh HR, Seco J, Flanz JB, Kooy HM. Golden beam data for proton pencil-beam scanning. Phys Med Biol. 2012;57(5):1147.
65. Paganetti H. Dose to water versus dose to medium in proton beam therapy. Phys Med Biol. 2009;54(14):4399.

66. Trofimov A, Unkelbach J, DeLaney TF, Bortfeld T. Visualization of a variety of possible dosimetric outcomes in radiation therapy using dose-volume histogram bands. Pract Radiat Oncol. 2012;2(3):164–71.
67. Clasie BM, Sharp GC, Seco J, Flanz JB, Kooy HM. Numerical solutions of the γ-index in two and three dimensions. Phys Med Biol. 2012;57(21):6981.
68. Giebeler A, Fontenot J, Balter P, Ciangaru G, Zhu R, Newhauser W. Dose perturbations from implanted helical gold markers in proton therapy of prostate cancer. J Appl Clin Med Phys. 2009;10(1):2875.
69. Devicienti S, Strigari L, D'Andrea M, Benassi M, Dimiccoli V, Portaluri M. Patient positioning in the proton radiotherapy era. J Exp Clin Cancer Res. 2010;29(1):1.
70. Veiga C, Janssens G, Teng C-L, Baudier T, Hotoiu L, McClelland JR, Royle G, Lin L, Yin L, Metz J, Solberg TD, Tochner Z, Simone CB, Mcdonough J, Teo B-KK. First clinical investigation of cone beam computed tomography and deformable registration for adaptive proton therapy for lung cancer. Int J Radiat Oncol Biol Phys. 2016;95(1):549–59.